HHS Public Access

Author manuscript

Cell Rep. Author manuscript; available in PMC 2021 August 17.

Published in final edited form as:

Cell Rep. 2021 July 27; 36(4): 109459. doi:10.1016/j.celrep.2021.109459.

In vivo isotope tracing reveals the versatility of glucose as a brown adipose tissue substrate

Su Myung Jung[1,4], **Will G. Doxsey**[1], **Johnny Le**[3], **John A. Haley**[1], **Lorena Mazuecos**[1], **Amelia K. Luciano**[1], **Huawei Li**[1], **Cholsoon Jang**[3,*], **David A. Guertin**[1,2,5,*]

[1]Program in Molecular Medicine, University of Massachusetts Medical School, Worcester, MA, USA

[2]Department of Molecular, Cell and Cancer Biology, University of Massachusetts Medical School, Worcester, MA, USA

[3]Department of Biological Chemistry, University of California Irvine, Irvine, CA, USA

[4]Department of Biological Sciences, Sungkyunkwan University, Suwon, South Korea

[5]Lead contact

SUMMARY

Active brown adipose tissue (BAT) consumes copious amounts of glucose, yet how glucose metabolism supports thermogenesis is unclear. By combining transcriptomics, metabolomics, and stable isotope tracing *in vivo*, we systematically analyze BAT glucose utilization in mice during acute and chronic cold exposure. Metabolite profiling reveals extensive temperature-dependent changes in the BAT metabolome and transcriptome upon cold adaptation, discovering unexpected metabolite markers of thermogenesis, including increased *N*-acetyl-amino acid production. Time-course stable isotope tracing further reveals rapid incorporation of glucose carbons into glycolysis and TCA cycle, as well as several auxiliary pathways, including NADPH, nucleotide, and phospholipid synthesis pathways. Gene expression differences inconsistently predict glucose fluxes, indicating that posttranscriptional mechanisms also govern glucose utilization. Surprisingly, BAT swiftly generates fatty acids and acyl-carnitines from glucose, suggesting that lipids are rapidly synthesized and immediately oxidized. These data reveal versatility in BAT glucose utilization, highlighting the value of an integrative-omics approach to understanding organ metabolism.

*Correspondence: choljang@uci.edu (C.J.), david.guertin@umassmed.edu (D.A.G.).

AUTHOR CONTRIBUTIONS

S.M.J., C.J., and D.A.G. conceptualized the study, designed the experiments, and interpreted the data. S.M.J. and W.G.D. performed all of the animal experiments and sample preparation with assistance from J.A.H., L.M., and H.L. C.J. and J.L. performed and analyzed MS experiments. A.K.L. performed insulin ELISA experiments. S.M.J., C.J., and D.A.G. analyzed and interpreted the data with assistance from W.G.D., J.L., and J.A.H. W.G.D. made the graphical abstract with assistance from S.M.J. S.M.J., C.J., and D.A.G. wrote the manuscript.

SUPPLEMENTAL INFORMATION

Supplemental information can be found online at https://doi.org/10.1016/j.celrep.2021.109459.

DECLARATION OF INTERESTS

The authors declare no competing interests.

Graphical abstract

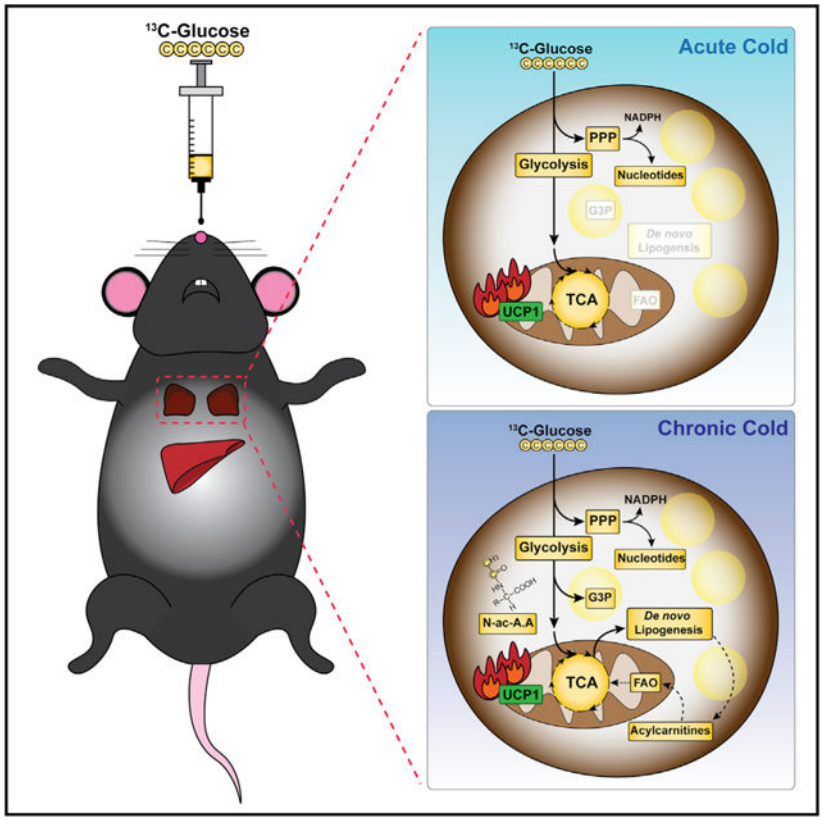

In brief

Jung et al. explore brown adipose tissue glucose utilization *in vivo* by metabolomics, stable isotope tracing, and transcriptomics data. They find extensive temperature-dependent changes in the BAT metabolome revealing several markers of thermogenesis and versatility in glucose utilization, including rapid coupling of *de novo* lipid and acyl-carnitine synthesis.

INTRODUCTION

Brown adipose tissue (BAT) is a mammalian organ specialized in transferring chemical energy into heat by a process called nonshivering thermogenesis (Cannon and Nedergaard, 2004). Newborn humans and rodents require BAT to protect body temperature against cold (Lidell et al., 2013), while small mammalian hibernators require BAT to withdraw from hypothermic torpor (Ballinger and Andrews, 2018). Certain diets also stimulate BAT in rodents living in their thermoneutral zone (i.e., in the absence of thermal stress) (Feldmann et al., 2009; Fischer et al., 2019; Hung et al., 2014; Jung et al., 2019; Rothwell and Stock, 1979; von Essen et al., 2017), suggesting BAT has metabolic functions beyond thermoregulation.

Non-shivering thermogenesis is mainly mediated by uncoupling protein 1 (UCP1), which uncouples the electron transport chain from ATP synthesis and thereby dissipates the

mitochondrial electrochemical proton gradient as heat. It is an energydemanding process associated with copious glucose uptake, similar to highly glycolytic tumors, making it readily detectable by ^{18}F-FDG PET (^{18}Fluorine-fluorodeoxyglucose positron emission tomography) imaging. This property enabled widespread detection of metabolically significant BAT deposits in the adult human population (Cypess et al., 2009; Nedergaard et al., 2007; Saito et al., 2009; van Marken Lichtenbelt et al., 2009; Virtanen et al., 2009) and launched a renaissance of interest in targeting BAT therapeutically to increase energy expenditure as a treatment for obesity and hyperglycemia. Thus, understanding how BAT uses glucose has important biological and clinical implications.

The metabolic fate of glucose in BAT has been inconclusive. Although it is often assumed that BAT directly metabolizes glucose via glycolysis and the tricarboxylic acid (TCA) cycle to provide fuel for thermogenesis (i.e., uncoupling), extensive evidence in the literature suggests other metabolic pathways fueled by glucose are also active during thermogenesis (Hankir and Klingenspor, 2018). For example, gene expression studies suggest that cold-activated BAT upregulates the pentose phosphate pathway (PPP), glycerol synthesis, and *de novo* lipogenesis (DNL) pathway, which are primarily fueled by glucose (Hao et al., 2015; Labbé et al., 2015; McCormack and Denton, 1977; Mottillo et al., 2014; Sanchez-Gurmaches et al., 2018; Shimazu and Takahashi, 1980; Trayhurn, 1979; Yu et al., 2002). Indeed, in the context of rat and more recently in humans, it was suggested that only a fraction of glucose may be used directly as fuel for thermogenesis (Isler et al., 1987; Ma and Foster, 1986; Saggerson et al., 1988; Weir et al., 2018; Yu et al., 2002), and that cold acclimation over several days increases ^{14}C glucose incorporation into lipid (Yu et al., 2002). Stable isotope tracing is beginning to be applied *in vitro* using cultured brown adipocytes to investigate this notion (Held et al., 2018; Panic et al., 2020; Winther et al., 2018); however, *in vivo* stable isotope tracing is required to understand glucose utilization in physiological contexts. Thus, the precise role of glucose in BAT under physiologically relevant environmental conditions, such as short- and long-term cold exposure or dietary stresses, remains largely unknown.

To systematically investigate BAT's glucose usage during cold exposure, we employed metabolomics and stable isotope tracing strategies coupled with transcriptomics analysis in mice chronically or acutely exposed to a cold environment. We provide *in vivo* evidence that glucose is a versatile BAT resource that supports a variety of metabolic functions beyond glycolysis and the TCA cycle, and that its function varies both with the duration and the degree of cold exposure. Our study establishes a framework for exploring BAT substrate utilization in various nutritional, genetic, and pathological states.

RESULTS

Cold exposure remodels the BAT metabolome

We first established parameters for performing metabolomics combined with stable isotope tracing in mice adapted to living at thermoneutrality (TN: 30°C), room temperature, which is mild cold for mice (MC: 22°C), or severe cold (SC: 6°C) for 4 weeks. Compared with mice living at TN or MC, those living in SC show slightly reduced body weight despite increased cumulative food intake (Figures S1A and S1B) consistent with increased

energy expenditure. As previously observed (Sanchez-Gurmaches et al., 2016, 2018), BAT mass increases by hypertrophy at TN relative to MC due to increased lipid accumulation, while mainly interscapular BAT (iBAT) mass also increases in SC relative to MC but by hyperplasia (Figures S1C and S1D). Both visceral perigonadal white adipose tissue (pgWAT) and posterior subcutaneous inguinal WAT (psWAT) decrease mass in SC (Figure S1C), which associates with increased formation of thermogenic adipocytes in scWAT (i.e., WAT browning) (Figure S1D). Liver mass increases with decreasing cold temperature with no obvious morphological differences by histology (Figures S1C and S1D). Western blotting confirms BAT UCP1 levels increase with cold (Figure S1E). Blood glucose levels are higher in SC-adapted mice in line with increased cumulative food intake (Figures S1B and S1F), while circulating insulin levels trend lower (Figure S1G), suggesting increased insulin sensitivity. These data confirm cold adaptation.

Using an *in vivo* glucose uptake assay, we confirmed that SC potently stimulates glucose uptake into BAT (Figure 1A). Next, to reflect physiological feeding, [U-^{13}C]-glucose tracer was provided via oral gavage in *ad libitum* fed mice across all three environmental conditions (Figure 1B). At 15, 30, and 60 min after providing tracer, the abundance and ^{13}C labeling of serum and BAT metabolites were measured by liquid chromatographymass spectrometry (LC-MS). Among the ~600 confirmed metabolites with authentic standards, we detected 433 metabolites in BAT, 125 of which are labeled from [U-^{13}C]-glucose (Figure S1H). Multivariate analysis by principal-component analysis clearly distinguishes each BAT metabolome by temperature (Figure 1C). Volcano plots show that the total number of significantly different metabolites between SC and TN (n = 177) is markedly greater than the number of different metabolites between MC and TN (n = 91) (Figures 1D and S1I). Thus, cold adaptation substantially remodels the BAT metabolome.

We found 73 metabolites that increase in both MC and SC (Figure S1J), including cyclic AMP, which is an intracellular second messenger required for BAT thermogenesis (Cannon and Nedergaard, 2004). Interestingly, cyclic AMP levels directly correlate with the degree of cold, confirming cyclic AMP as a thermogenic reporter (Figure 1E). We find 30 additional metabolites that exhibit similar profiles, including *N*-acetyl-serine, ribose phosphate, acyl carnitines, glycero-lipids, and uric acid (Figure 1E; Table S1), suggesting several metabolite reporters of thermogenesis.

Pathway impact analysis reveals unexpected metabolic pathways activated by SC, including arginine biosynthesis, pyrimidine metabolism, aminoacyl-tRNA biosynthesis, glutathione (GSH) metabolism, and pantothenate/coenzyme A (CoA) biosynthesis (Figure 1F). GSH metabolism and PPP are also activated by MC, as is the nicotinate/nicotinamide pathway (Figure S1K). Several groups of similar metabolites show increased abundance upon cold, including *N*-acetylated amino acids, acyl carnitines, and glycerol-lipids (see red highlights in Figure S2). The complete dataset of whole metabolome is in the supplemental information (Data S1 and S2). These data uncover many metabolic pathways not previously associated with thermogenesis that show dynamic changes upon cold adaptation.

Cold differentially regulates upper and lower glycolysis

Next, we integrated the metabolomics and [U-^{13}C]-glucose tracing data with BAT RNA sequencing data that we generated using age-, sex-, and strain-matched mice under identical environmental conditions (Sanchez-Gurmaches et al., 2018). A recent *in vitro* systematic ^{13}C-glucose tracing study in cultured baby mouse kidney cells overexpressing each glycolysis enzyme identified four critical glycolytic flux control steps that can be regulated by protein expression level: glucose import, hexokinase, phosphofructokinase, and lactate export (Tanner et al., 2018). We find that transcription of the glucose transporters *Glut1* and *Glut4* does not significantly change upon cold (Figure 2A), although glucose transporters may be regulated by protein stability and/or membrane trafficking, which were not examined. SC markedly upregulates upper glycolytic enzymes (*Hk1*, *Gpi*, *Pfkl*, *Pfkp*) and lower glycolytic enzymes (*Aldoa*, *Gapdh*, *Pgam1*, *Eno1*) (Figures 2A and 2B). Interestingly, *hexokinase* seems to undergo isozyme switching from *Hk2* to *Hk1* in SC (Figure 2A). *Pgam1* and *Pgam2*, as well as *Eno1*, *Eno2*, and *Eno3*, show a similar isozyme switching pattern (Figure 2B). Conversely, the lactate transporters *monocarboxylate transporter 2* (*Mct2*) and *Mct4* decrease in expression in cold (Figure 2C). Thus, glycolysis is transcriptionally induced by SC adaptation.

Gene expression changes upon MC adaptation were less striking (Figures 2A-2C), suggesting upper glycolytic flux may be driven by additional mechanisms in MC, such as insulin action, which increases in MC relative to TN based on AKT phosphorylation (Jung et al., 2019; Sanchez-Gurmaches et al., 2018). In contrast, AKT phosphorylation decreases in SC relative to MC(Jung et al., 2019; Sanchez-Gurmaches et al., 2018). Thus, transcriptional regulation of BAT glycolytic enzymes may be more critical for driving glycolytic fluxes in SC.

We next examined glucose carbon usage by BAT by [U-^{13}C]-glucose tracing. Because BAT metabolome pool sizes markedly change upon cold exposure (Figures 1C and 1D), we measured the abundance of total labeled metabolites, rather than labeling fractions that are affected by metabolites' pool sizes. We also measured at multiple time points (15, 30, and 60 min after providing tracer) to capture the kinetics and total amount of glucose carbon fluxes into metabolic pathways. After providing the tracer, mice at TN show modestly slower glucose excursion and clearance in blood (Figure S3A). In BAT, however, the labeled glucose level is strikingly lower in SC compared with warmer temperatures (Figure S3B). We interpret this as immediate glucose catabolism given that SC BAT shows a large increase in glucose uptake (Figure 1A). Consistent with this notion, SC BAT exhibits robust labeling of glycolytic intermediates within 15 min of gavage; for example, F1,6BP and lactate increase over 3-fold compared with TN, while fructose 6-phosphate/glucose 6-phosphate, glyceraldehyde 3-phosphate, 3-phosphoglycerate, phosphoenolpyruvate, and pyruvate increase between 1.8-fold and 2.4-fold (Figures 2D-2J and S3C). MC similarly increases the labeling of F1,6BP (2-fold within 15 min) relative to TN; however, downstream glycolytic intermediate labeling is unchanged (Figure 2D-2J). Both SC and MC increase glucose labeling of glycerol 3-phosphate, a precursor to glycerol (Figure S3D), and this correlates with increased expression of the *glycerol-3-phosphate dehydrogenase* enzymes *Gpd1* and *Gpd2* (Figure S3E), additionally suggesting that cold-induced glucose

flux through glycolysis feeds glycerol synthesis (Figure 2K). In comparison, liver shows reduced glucose uptake and decreased glycolytic intermediates labeling from ^{13}C-glucose (Figures 1B and S3F-S3K). Overall, these data indicate that the degree of cold differentially accelerates upper and lower glycolytic flux in BAT.

BAT uses glucose to support auxiliary pathways branching from glycolysis

Glucose carbons can branch from glycolysis into PPP, which we identified as cold activated by unbiased pathway analysis (Figures 1F and S1K). Consistently, SC-adapted BAT shows upregulation of PPP genes (Figure S4A) and rapid labeling of PPP intermediates (6-PG and S7P) from ^{13}C-glucose (Figures 3A-3C). One primary function of the PPP is to provide cytosolic NADPH, which is used in many anabolic reactions, such as lipid and nucleic acid synthesis. Indeed, the NADPH level and the NADPH/NADP$^+$ ratio are highly increased by SC (Figures 3D and 3E). This increased NADPH may support increased production of antioxidant glutathione (GSH) (Figures 3F and S4C), which might additionally serve as a countermeasure to oxidative stress resulting from cold-induced mitochondrial uncoupling (Shabalina and Nedergaard, 2011). The role of oxidative stress in BAT thermogenesis is just beginning to be understood (Chouchani et al., 2019).

The PPP pathway also provides ribose for nucleotide biosynthesis. Interestingly, SC-adapted BAT shows accelerated glucose carbon incorporation into ribose-phosphate (R5P/R1P) and deoxyribose-phosphate (Figures 3A, 3G, and 3H). SC also induces glucose carbon usage for purine and pyrimidine metabolites, including inosine monophosphate, guanosine diphosphate, Orotate, and uridine monophosphate (Figures 3A and 3I-3N). Surprisingly, however, SC markedly decreases gene expression of the purine/pyrimidine synthesis pathway (Figures S4D and S4E). This inverse relationship may reflect negative feedback regulation (Ben-Sahra et al., 2013).

Transient SC adaptation reportedly activates purine breakdown by increasing expression of *guanosine monophosphate reductase* (*Gmpr*; GMP-degrading enzyme) and *adenosine monophosphate dehydrogenase* (*Ampd*; AMP-degrading enzyme) (Fromme et al., 2018; Salvatore et al., 1998). Consistently, *Gmpr* and *Ampd3* transcription also increases in SC adaptation, while *Ampd1/Ampd2* decreases (Figure S4F). SC increases the purine nucleoside monophosphates AMP and GMP, as well as their degradation products xanthine, xanthosine, and uric acid (Figures S4G-S4N). This suggests both increased purine synthesis and degradation in SC-adapted BAT. Other glycolysis branching pathways, including glycogen and hexosamine synthesis, did not exhibit consistent labeling trends, although the *phosphoglucomutase 2* (*Pgm2*), *UDP-glucose pyrophosphorylase* 2 (*Ugp2*), *glycogen synthase 2* (*Gys2*), and *glycogen phosphorylase L* (*Pygl*) genes involved in glycogen synthesis and breakdown increase expression in cold (Figures S5A-S5F). Collectively, SC-adapted BAT uses glucose carbons to support the PPP and nucleotide synthesis in addition to glycolysis (Figure 3O).

SC, but not MC, adaptation increases glucose flux into the TCA cycle

We next investigated glucose incorporation into the TCA cycle, the primary pathway for producing NADH that fuels mitochondrial uncoupling. Both MC and SC increase

transcription of mitochondrial pyruvate carriers (MPCs) and pyruvate dehydrogenases (PDHs) that stimulate glucose carbon entry into mitochondria (as pyruvate) and its entry into the TCA cycle (as acetyl-CoA) (Figure 4A). Ironically, cold also increases PDH kinases (PDKs) that inhibit PDH activity (Figure 4B). Cold has minimal effects on TCA cycle enzyme transcription, with no genes showing greater than 2-fold induction (Figure 4C). Thus, BAT TCA cycle gene expression changes are largely refractory to cold adaptation.

Despite minimal gene expression changes, ^{13}C-glucose tracing reveals significant glucose carbon entry into the BAT TCA cycle, but only in SC (Figures 4D-4H). Although MC potently induces thermogenesis (because this is below the thermoneutral zone for mice) (Gordon, 2012; Nedergaard et al., 2011), MC shows only a trending increase in glucose carbon entry into the TCA cycle (Figures 4D-4I). This suggests that BAT may preferentially uses other substrates, such as fatty acids and/or glutamine, to fuel the TCA cycle in MC.

Plotting the labeling over time shows that total glucosederived carbons entering TCA cycle intermediates (i.e., citrate, malate, succinate, aconitate) are profoundly elevated (~6-fold) in SC within 15 min of providing tracer. Intriguingly, the labeling of TCA cycle intermediate is greater than that of glycolytic intermediates in BAT (Figures 4I and 4J), suggesting glucose carbons can also enter the TCA cycle indirectly through non-glycolytic metabolites. One potential source is circulating TCA intermediates. However, serum-labeled TCA intermediates do not match with BAT TCA intermediates, except for succinate (Figures S6A-S6C), and their labeled levels in serum are ~50- to 200fold lower than those in BAT (Figure S6D). Furthermore, in the liver, which can provide circulating TCA intermediates, we observed rather decreased TCA labeling by cold acclimation (Figures S6E-S6I). This is consistent with reduced hepatic glucose uptake and glycolysis labeling upon cold adaptation (Figures 1B and S3F-S3K). Thus, the contribution of circulating TCA intermediates to the BAT TCA cycle is likely insignificant.

The TCA cycle can be also fueled by circulating lactate made from glucose (Hui et al., 2017). Labeled serum lactate levels are comparable among the groups (Figure S6J), but significantly lower (~4-fold) than in BAT (Figure S6K). Moreover, the observation that SC markedly increases BAT lactate labeling along with glycolytic intermediates rather than circulating lactate (Figure 2) suggests BAT preferentially uses circulating glucose rather than lactate to feed the TCA cycle. Glutamine, another abundant circulating nutrient, and its cousin glutamate show robust labeling from glucose in BAT (Figures 4K and 4L), raising the possibility that circulating glutamine may feed the BAT TCA cycle (Cluntun et al., 2017). We did observe increased glutamine and glutamate labeling in the liver and serum at the 15-min time point (Figure S6L-S6O), but their labeled serum levels are 15-fold and 380-fold lower than in BAT (Figures S6P and S6Q). Thus, glutamine in BAT is likely produced from glucose within BAT. Together, while circulating metabolites generated from other organs may contribute to the BAT TCA cycle, most glucose carbons entering the BAT TCA cycle are primarily from glycolysis (Figure 4M).

SC rapidly couples BAT fatty acid synthesis and oxidation

Citrate is among the TCA cycle intermediates most highly labeled from glucose in SC (by ~8-fold) (Figure 4J). Moreover, the mitochondrial citrate carrier (*Slc25a1*) exporting

citrate to the cytosol increases 5-fold in cold (Figure S7A). Cytosolic citrate is converted to acetyl-CoA in the first step of DNL. Consistently, both MC and SC potently induce the DNL enzymes *Acly*, *Acc*, and *Fasn* in BAT (Figures S1E and S7A) (Sanchez-Gurmaches et al., 2018) in addition to increasing D_2O labeling of newly synthesized lipids (Sanchez-Gurmaches et al., 2018; Trayhurn, 1981). The rise in NADPH production through the PPP (Figure 3D) would support DNL. ^{13}C-glucose tracing demonstrates that SC accelerates glucose-driven synthesis of the lipogenic precursors acetyl-CoA and malonyl-CoA and of the fatty acids myristate (C14:0), palmitate (C16:0), palmitoylate (C16:1), and stearic acid (C18:0) (Figures 5A-5G). Interestingly, although MC BAT increases the DNL pathway and lipid D_2O labeling (Sanchez-Gurmaches et al., 2018), it does not increase ^{13}C-glucose incorporation into fatty acids (Figures 5A-5G and S7A-S7C). Thus, MC BAT may utilize other substrates for DNL, such as glutamine or acetate (Luong et al., 2000; Ouellet et al., 2012; Sanchez-Gurmaches et al., 2018; Yoo et al., 2008), or take up circulating lipids synthesized by the liver. However, the ^{13}C-glucose-labeled fatty acids in BAT are >100-fold higher in total abundance and show ~10^7-fold higher labeling than in serum (Figures 5H and S7D-S7I), indicating they are likely endogenously produced.

Strikingly, SC BAT also labels numerous acyl-carnitine species (short-, medium-, and long-chain acyl-carnitines) within 15 min of providing ^{13}C-glucose (Figures 5A and 5I-5L). This is consistent with the induction of genes involved in acyl-carnitine production and transport, such as *Aacs* (*Acetoacetyl-CoA synthetase*), *Acsl3* (*Acyl-CoA synthetase long chain family member 3*), *Acsl5* (*Acyl-CoA synthetase long chain family member 5*), and *Cpt2* (*Carnitine palmitoyl transferase 2*) (Figure S7J). In contrast, serum acyl-carnitine levels or labeling are not altered by cold (Figures S7D and S7K-S7P), and their abundance is negligible compared with BAT (Figures 5M and S7Q). This indicates remarkably rapid *de novo* acyl-carnitine synthesis (reflecting fatty acid oxidation; Figure S7R) coupled with fatty acid synthesis upon SC adaptation for efficient energy production and lipid synthesis (Figure 5N).

Glucose contributes to the phosphatidyl-glycerol (PG) pool

Lipidomics analysis reveals that a variety of PG species are also rapidly and robustly labeled from ^{13}C-glucose in SC and to a lesser extent in MC (Figures S8A-S8F). Intriguingly, glucose labeling appears specific for PG synthesis because other abundant phospholipids such as phosphatidyl-ethanolamine (PE) or phosphatidyl-serine (PS) do not show distinguishable changes upon cold adaptation (Figures S8A and S8G-S8I). This may reflect that the glycerol moiety of PG is derived from glucose. PG is a precursor of cardiolipin, which is important for mitochondrial phospholipid synthesis and required for optimum thermogenesis (Lynes et al., 2018; Sustarsic et al., 2018). Consistently, cold increases the cardiolipin synthesis genes *Pgs1* and *Crls1* in BAT (Figure S8J). SC also increases many types of lyso-phospholipid species, but without significant labeling from glucose (Figures S8A and S8K-S8M). Collectively, cold-adapted BAT seems to use glucose to increase PG production and likely cardiolipin to support mitochondrial membrane synthesis and function (Figure S8N).

Cold-adapted BAT uses glucose to generate *N*-acetyl-amino acids (N-Ac-AAs)

Among the 125 BAT metabolites labeled from glucose, 12 of them (~10%) are N-Ac-AAs (Figures 6A-6J). Their pool size increases with decreasing temperature (Figure 6A), and some show greatly enriched pool size in BAT relative to blood (e.g., ~4,000-fold for *N*-acetyl-glutamate) (Figure 6B). These N-Ac-AAs can be subdivided by their distinct labeling patterns. For example, only SC induces rapid but transient glucose carbon incorporation into *N*-acetyl-aspartate, *N*-acetyl-asparagine, *N*-acetyl-cysteine (NAC), and *N*-acetyl-methionine (Figures 6C-6F). In contrast, both SC and MC induce gradual glucose carbon accumulation in *N*-acetyl-glutamate, *N*-acetyl-glutamine, *N*-acetyl-serine, and *N*-acetyl-threonine (Figures 6G-6J). Most show M+2 labeling (i.e., only two carbons are labeled), suggesting that the 2-C acetyl moiety is generated from ^{13}C-glucose (Figures S9A-S9H). The abundance of specific N-Ac-AA species in BAT, but not in circulation, suggests potential physiological roles that require further investigation.

BAT uses glucose differently during acute cold exposure

Understanding how BAT uses glucose under different conditions is important to realizing its therapeutic potential as a glucose sink. Moreover, studies inconsistently use acute and chronic cold exposure experiments to test the functionality of BAT-mediated thermogenesis in defending body temperature. Whereas prolonged cold exposure reflects an adaptive condition in which BAT becomes optimized for maximum thermogenic efficiency, acute cold exposure is a sudden emergency in which protective measures extending beyond those provided by BAT (e.g., increased shivering) contribute to defense against hypothermia. We hypothesized that BAT may use glucose differently upon acute cold versus chronic cold exposure. To test this, we performed ^{13}C-glucose tracing in mice acutely exposed to SC for 5 h. During acute cold exposure, BAT mass tends to decrease as a result of a decrease in lipid droplet size, while the mass and histology of other tissues examined are unchanged (Figures S10A-S10C). UCP1 levels are also unperturbed by acute cold exposure (Figure S10D), consistent with increased BAT thermogenesis being driven mainly by substrate mobilization and/or posttranslational stimulation under these conditions. Serum glucose and insulin levels also tend to increase after acute cold exposure (Figures S10E and S10F) (Heine et al., 2018).

Glucose uptake assays using [^{3}H]-2DG show that BAT increases glucose uptake by ~2-fold upon acute cold exposure (Figure 7A). After ^{13}C-glucose administration (Figure 7B), acute cold-exposed mice show lower glucose labeling but higher labeling of most glycolytic intermediates in BAT than control mice (Figures 7C-7E and 7O), suggesting increased glycolysis flux. Intriguingly, we also observed lower R5P/R1P labeling but higher labeling of pyrimidine metabolites, such as AMP and IMP, suggesting that increased glucose utilization for nucleotide synthesis through the PPP also occurs during acute cold exposure (Figures 7F-7H). Moreover, TCA cycle intermediates and glutamine/glutamate labeling from glucose increases, which is also similar to the BAT from cold-adapted mice (Figures 7I-7K and 7O). However, there is no increase in fatty acid labeling from ^{13}C-glucose (Figures 7O and S10G-S10J), suggesting glucose carbons entering the mitochondria via pyruvate and converted to acetyl-CoA may be mainly used for oxidation. Thus, the glucose-

driven fatty acid synthesis-fatty acid oxidation pathway appears to be a unique metabolic reprogramming event occurring with prolonged cold exposure.

DISCUSSION

A key advance of our study is the comprehensive elucidation of temperature-driven changes in the metabolic fate of glucose by BAT *in vivo* by stable isotope tracing. Importantly, we uncovered metabolite markers of thermogenesis, including specific N-Ac-AAs, and cold-stimulated metabolic pathways not previously linked to thermogenesis. We also differentiate between BAT glucose utilization during acute cold exposure and chronic cold adaptation, which reveals a sharp distinction with rapid glucose-driven lipid synthesis being a unique hallmark of BAT metabolism in cold-adapted mice. These data suggest potential avenues of BAT biology that merit further investigation, especially in humans, because this may help elucidate how BAT could function as a nutrient sink.

The identification of N-Ac-AAs as thermogenic markers was particularly interesting. One possible function is that they buffer acetyl-CoA levels for lipogenesis or protein lysine acetylation. In fact, recent studies suggest that brown adipocytes synthesize *N*-acetyl-aspartate (by aspartate *N*-acetyl transferase) in a pathway previously thought to have a brain-specific role in providing acetyl-CoA precursors for lipid synthesis and myelin integrity (Chakraborty et al., 2001; Huber et al., 2019; Pessentheiner et al., 2013; Prokesch et al., 2016). Alternatively, N-Ac-AAs may function as a sink for two carbon units, which may facilitate CoA recycling for fatty acid oxidation (Allred and Guy, 1969). Cold-induced BAT proteasomal activity (Bartelt et al., 2018) raises the possibility that some N-Ac-AAs could derive from the degradation of N-terminally (α-amino group) acetylated or lysine-acetylated (ε-amino group) proteins (Aksnes et al., 2019; Arnesen, 2011). These possibilities are not necessarily mutually exclusive. NAC and *N*-acetyl-glutamate are the most upregulated N-Ac-AAs (Figures 6A, 6E, and 6H). NAC is renowned for its antioxidant properties (Kerksick and Willoughby, 2005), and systemic NAC administration improves metabolic fitness (Straub et al., 2019; Williams et al., 2019). *N*-acetyl-glutamate stimulates the urea cycle, which is thought to be liver specific but may have a role in BAT (Ramirez et al., 2017). These possibilities need further investigation.

Although thermogenesis is driven by lipid catabolism and mitochondrial substrate oxidation, our data and other previous studies suggest BAT paradoxically increases the anabolic DNL pathway (McCormack and Denton, 1977; Mottillo et al., 2014; Sanchez-Gurmaches et al., 2018; Shimazu and Takahashi, 1980; Townsend and Tseng, 2015; Trayhurn, 1979; Yu et al., 2002). This is further supported by recent evidence showing BAT fatty acid synthesis and oxidation genes oscillate with similar circadian rhythms in the cold (Adlanmerini et al., 2019). This appears to be an adaptation to prolonged cold exposure that is likely necessary for optional thermogenesis. Why BAT couples fatty acid synthesis and oxidation remains unknown but may provide an additional UCP1-independent futile cycle that contributes to thermogenesis, such as the recently described creatine substrate and calcium cycling pathways (Ikeda et al., 2017; Kazak et al., 2015, 2017).

It is also interesting to consider how BAT is capable of running lipid synthesis and oxidation simultaneously. For example, malonyl-CoA is well known to allosterically inhibit CPT1 to prevent fatty acid oxidation and synthesis from occurring simultaneously (Hue and Taegtmeyer, 2009). It is possible that mitochondrial heterogeneity exists within brown adipocytes as recently suggested (Benador et al., 2018; Yu et al., 2015), with some favoring lipid anabolism and others lipid catabolism (Benador et al., 2019). Alternatively, fatty acid synthesis and oxidation may occur in different adipocytes because lineage tracing and single-cell RNA sequencing suggest heterogeneous pools of brown adipocytes may also exist (Sanchez-Gurmaches et al., 2016; Song et al., 2020; Sun et al., 2020). We also observe increased glucose labeling of short-chain acyl-carnitine and medium-chain acyl-carnitine species (Figures 5A, 5I, and 5J) in SC BAT, which can enter mitochondria independent of CPT1 (McDonnell et al., 2016; McGarry and Foster, 1971). These could be pre-generated in the peroxisome; indeed, BAT peroxisome genes and activity are upregulated in SC (Nedergaard et al., 1980; Sanchez-Gurmaches et al., 2018). Given the rapid turnover of glucose-labeled malonyl-CoA (Figure 5C), it may not accumulate under these conditions, or BAT may preferentially generate malonyl-CoA through ACC1, which is mainly used for fatty acid synthesis, rather than ACC2, which generates malonyl-CoA at the mitochondrial membrane that is preferentially utilized for CPT1 inhibition (Wakil and Abu-Elheiga, 2009). Additional genetic and biochemical studies are required to understand the significance of flux into DNL.

There are some limitations of our study. First, tissue heterogeneity cannot be accounted for. Endothelial cells, neurons, immune cells, and brown adipocyte precursors may constitute 60%–70% of whole BAT tissue, and their individual contributions to the observed metabolic fluxes cannot be delineated (Scheele and Wolfrum, 2020). Second, the precise flux of glucose (i.e., mmol/min/kg) that enters into BAT from circulation and into specific metabolic pathways is not quantified. To measure these fluxes, constant isotopic infusion of ^{13}C-glucose and other tracers with quantitative analyses that account for inter-conversion of circulating metabolites is required (Hui et al., 2020; Jang et al., 2018). Nevertheless, our systems-level isotope tracing analysis paired with transcriptomics and metabolomics reveals a systems-level view of BAT glucose carbon usage *in vivo* in three different temperatures. These strategies can be applied to examining glucose or other nutrient utilization in diverse physiological, genetic, pathological states, or sex because the effect of gender on BAT glucose utilization has not been determined (Hankir and Klingenspor, 2018; Olsen et al., 2017).

Our data collectively suggest a model in which BAT utilizes glucose differently depending upon the degree and duration of cold exposure, and that glucose is used to support multiple auxiliary processes beyond glucose/TCA cycle metabolism. Interestingly, a recent glucose tracing study in cold-adapted BAT shows no increase in glycolysis and fatty acid labeling from glucose (Wang et al., 2020); however, a variety of reasons can explain these differences. First, Wang et al. (2020) used 10-day cold acclimation followed by intraperitoneal injection of glucose and measured fractional labeling of metabolites. In contrast, we use 4-week cold acclimation with oral delivery of glucose tracer and report total labeled carbons for each metabolite. This is because we observe greater than 40% of the whole BAT metabolome (including glycolysis, PPP, fatty acids, and lipids) increasing

in abundance (≥2-fold) upon SC (Figure 1D). This increased pool size dilutes the labeling faction despite the increased fluxes. Our findings are consistent with earlier *in vitro* studies suggesting active brown adipocytes oxidize only ~2%–16% of the glucose consumed for energy production in the TCA cycle (Hankir and Klingenspor, 2018; Isler et al., 1987; Ma and Foster, 1986). However, the rapid coupling of lipid synthesis and acyl-carnitine production and increased labeling of glutamine/glutamate by ^{13}C-glucose with cold suggests glucose may additionally take indirect routes to being oxidized. Notably, MC does not appear to increase glucose disposal by directly increasing its flux into the TCA cycle for oxidation. This may be an important consideration when developing therapeutic strategies that mimic cold activation.

A recent study using a microdialysis infusion method reports increased glucose uptake and lactate release from human BAT upon cold exposure (Weir et al., 2018). These data are consistent with our findings as we observe higher glucose uptake and robust lactate labeling in the BAT of cold-adapted mice (Figure 2). This study also noted that cold increases BAT glutamate uptake. In contrast, our data suggest BAT may produce glutamate autonomously using glucose (Figures 4 and S6). The discrepancy could relate to methodology and/or species difference between the studies. Future isotope tracing studies using steady-state infusion combined with arterio-venous metabolomics will enable us to better understand which nutrients are produced or released by BAT and how they are metabolized.

STAR★METHODS

RESOURCE AVAILABILITY

Lead contact—Further information and request for resources and reagents should be directed to and will be fulfilled by the lead contact, David A. Guertin (david.guertin@umassmed.edu).

Materials availability—This study did not generate new unique reagents

Data and code availability

Data availability: Raw dataset of isotope tracing and metabolomics generated during this study have been deposited at supplemental information (Data S1 and S2) and listed in the key resources table. This paper analyzes existing, publicly available data (RNA-seq). The accession number for the dataset is listed in the key resources table.

Code availability: This paper does not report original code.

Post-publication availability of data and code: Any additional information required to reanalyze the data reported in this paper is available from the lead contact upon request.

EXPERIMENTAL MODEL AND SUBJECT DETAILS

Mice—All 10-weeks old wild-type C57Bl6/J male mice were used in this study were purchased from Jackson laboratory (Cat#000664). Mice were housed in the UMMS Sherman Center Animal Medicine Facility in a clean room set at 22°C and 45% humidity on

a daily 12h light/dark cycle (7 AM to 7 PM), and placed in ventilated racks fed *ad libitum* with a standard chow diet (LabDiet Cat#RMH3000; 60% Carbohydrate, 26% Protein, 14% Fat), with bedding changed every two weeks. Mice were sacrificed at 10-14 weeks old depending on the experiment. Please refer to figure legends for further details. All animal experiments were approved by the University of Massachusetts Medical School Institutional Animal Care and Use Committee.

METHOD DETAILS

Temperature Acclimation Experiment—For temperature adaptation to either thermoneutrality (30°C) or severe cold (6°C), 10-weeks old wild-type C57Bl6/J male mice were housed for 4-weeks in two-rodent incubators (RIT33SD, Powers Scientific) located in UMMS Sherman Center Animal Medicine Facility with standard housing conditions aforementioned in Mice section except housing temperature. One rodent incubator had the temperature set to 30°C (thermoneutrality group). Another incubator started to set at 18°C, followed by decreasing 4°C weekly until reaching at 6°C which temperature the mice stayed for a week (severe cold group). Mild cold (22°C) group mice were co-housed with same conditions as the mice in rodent incubators. Cages including beddings, food and water but no enrichments for nesting were pre-adjusted to corresponding temperatures at least 24-hour before the cage set up and replaced every week. Body weight and food intake were monitored weekly for four weeks.

Acute Cold Challenge—10-weeks old wild-type C57Bl6/J male mice were transferred early in the morning to prechilled cages in a 6°C cold room with free access to pre-chilled food and water. Beddings but no enrichments for nesting were included in cage. Rectal temperature was measured hourly using a rectal probe (RET-3, ThermoWorks).

Histological Studies—Samples from adipose tissue depots, liver and muscle were fixed in formalin (3.7% in 90% ethanol) for 24 h and were embedded in paraffin. After sectioning, hematoxylin / eosin (HE) staining was performed using standard protocols.

Western Blot Analysis—For immunoblot analysis of surgically dissected brown adipose tissue depots, tissues were homogenized and lysed in RIPA buffer (150 mM NaCl, 50 mM HEPES at pH 7.4, 0.1% SDS, 1% Triton X-100, 2 mM EDTA, 0.5% Na-deoxycholate) containing a protease and phosphatase inhibitor cocktail. Protein lysates were mixed with 5X SDS sample buffer and boiled, separated by SDS-PAGE, transferred to polyvinylidene difluoride (PVDF) membrane filters, and subjected to immunoblot analysis.

Blood Glucose and Insulin Measurements—Blood glucose levels were measured by tail bleeding with a commercially available glucose meter. (Bionime, GE100 Glucose meter) Serum insulin levels were determined using commercial kits according to the manufacturer's instructions (Crystal Chem, Cat #90060).

***In vivo* Glucose Uptake Assay—**^{3}H-deoxyglucose (^{3}H-2DG;[1,2-3H(N)]-Deoxy-D-glucose, NET328A001MC, Perkin Elmer) was used to evaluate glucose uptake into brown adipose tissue (BAT), subcutaneous adipose tissue (SAT, inguinal WAT), visceral adipose

tissue (VAT), liver and quadricep as previously described in (Jung et al., 2019) with minor modifications. Briefly, mixture of ^{3}H-2DG (17 μCi/Kg) and unlabeled glucose (1g/Kg) was prepared as solutions in normal saline (0.9% NaCl). Mice *ad lib* from 4-week of temperature acclimation to 30°C, 22°C and 6°C were fed the ^{3}H-DOG/glucose mixture solution (10 μL/g body weight) through oral gavage using plastic feeding tube (Instech Laboratories, Plymouth meeting, MA). An hour following the gavage, organs and blood from anesthetized mice were harvested. Specific fractional uptakes of ^{3}H-DOG were determined using a scintillation counter (liquid scintillation analyzer Tri-Carb2900TR, PerkinElmer, Montreal, QC, Canada).

***In vivo* Isotope Tracing and Sample Collection—**Mice from 4-week of temperature acclimation to 30°C, 22°C and 6°C were used. Prior to isotope delivery, blood samples (~20 μL) were collected by tail bleeding for 0 min time point. Then, mice were fed (10 μL/g body weight) normal saline solution containing [U-^{13}C]-glucose (1g/kg, CLM-1396-PK, Cambridge Isotope Laboratories) using plastic feeding tube. After 15, 30 and 60 minutes from feeding, mice were euthanized and blood (~100 μL) were collected through cardiac puncture and tissues were quickly dissected and snap frozen (< 5 s) in liquid nitrogen with a pre-cooled Wollenberger clamp (Wollenberger et al., 1960). For serum, blood samples were placed on ice in anticoagulant-free tube for 20 min, followed by centrifugation at 16,000 x g for 10 min at 4°C. The resulting supernatant was stored in −80°C. Whole BAT and liver were harvested and grounded to homogeneous powder using a Cryomill (Retsch, Newtown, PA) and stored in −80°C before metabolite extraction. During the entire experimental procedures before euthanasia, all mice were tightly kept being acclimated in their own group's temperature.

Metabolite Extraction—To extract metabolites from serum samples, 150 μL of methanol was added to 5 μL of serum sample and incubated on ice for 10 min, followed by vortexing and centrifugation at 16,000 x g for 10 min at 4°C. The supernatant (3 μL) was loaded to LC-MS. To extract metabolites from tissue samples, tissue powder was weighed (~20 mg) on dry ice. The extraction was done by adding −20°C methanol:acetonitrile:water (40:40:20) mixture to the powder, followed by vortexing and centrifugation at 16,000 x g for 10 min at 4°C. The volume of the extraction solution (mL) was 40 x the weight of tissue (mg) to make an extract of 25 mg tissue per mL solvent. The supernatant (3 μL) was loaded to LC-MS.

LC-MS—Samples were analyzed using a quadrupole-orbitrap mass spectrometer (Q Exactive Plus, Thermo Fisher Scientific, San Jose, CA) operating in negative or positive ion modes, coupled to hydrophilic interaction chromatography via electrospray ionization and used to scan from m/z 70 to 1000 at 1 Hz and 140,000 resolution. LC separation was on a XBridge BEH Amide column (2.1 mm x 150 mm, 2.5 mm particle size, 130A° pore size) using a gradient of solvent A (20mM ammonium acetate, 20mM ammonium hydroxide in 95:5 water: acetonitrile, pH 9.45) and solvent B (acetonitrile). Flow rate was 150 ml/min. The LC gradient was: 0 min, 85% B; 2 min, 85% B; 3 min, 80% B; 5 min, 80% B; 6 min, 75% B; 7 min, 75% B; 8 min, 70% B; 9 min, 70% B; 10 min, 50% B; 12 min, 50% B; 13 min, 25% B; 16 min, 25% B; 18 min, 0% B; 23 min, 0% B; 24 min, 85% B; 30 min, 85% B. Autosampler temperature was 4°C. Data were analyzed using the MAVEN software

(Melamud et al., 2010). Isotope labeling was corrected for natural 13C abundance using AccuCor (Su etal., 2017).

RNA Sequencing Data Analysis—Previously deposited RNA-sequencing data that were re-analyzed here are available under access codes [GSE96681] (Sanchez-Gurmaches et al., 2018). Transcriptomic abundance is presented via relative counts per million (CPM). Differential gene expression analysis among three temperature groups were generated such that CPM is normalized such that thermoneutrality (30°C) group's CPM = 1.

QUANTIFICATION AND STATISTICAL ANALYSIS

Data are presented as mean + SEM or mean ± SEM, unless stated otherwise. Student's t test or analysis of variance (ANOVA; one or two ways) were used to determine statistical significance for two groups or three groups, respectively. Statistical analysis was done using GraphPad Prism. $p < 0.05$ was considered statistically significant. The statistical parameters (i.e., number of mice used per experiment, *P*-values) are stated in each figure legend.

Supplementary Material

Refer to Web version on PubMed Central for supplementary material.

ACKNOWLEDGMENTS

We thank the Guertin lab and Jang lab members for valuable discussions. We also thank Dr. Joshua Rabinowitz for supporting LC-MS use and Camila Martinez Calejman for technical assistance. This work was supported by National Institutes of Health (NIH) grants R01DK094004, R01CA196986, and R01DK116005 (to D.A.G.); American Association for the Study of Liver Disease (AASLDF 50028) and Edward Mallinckrodt, Jr. Foundation grants (to C.J.); and NIHMS of the National Institutes of Health grant number T32GM008620 (to J.L.). S.M.J. was supported by a postdoctoral fellowship from the American Diabetes Association (1-18-PDF-128). L.M. was supported by an International Grant for stays in Universities and Research Centers from UCLM Own Research Plan co-financed by European Development Fund Regional (FEDER, Reference DOCM 204). A.K.L. is supported by a post-doctoral fellowship from the American Cancer Society (PF-19-103-01-TBE).

REFERENCES

Adlanmerini M, Carpenter BJ, Remsberg JR, Aubert Y, Peed LC, Richter HJ, and Lazar MA (2019). Circadian lipid synthesis in brown fat maintains murine body temperature during chronic cold. Proc. Natl. Acad. Sci. USA 116, 18691–18699. [PubMed: 31451658]

Aksnes H, Ree R, and Arnesen T (2019). Co-translational, Post-translational, and Non-catalytic Roles of N-Terminal Acetyltransferases. Mol. Cell 73, 1097–1114. [PubMed: 30878283]

Allred JB, and Guy DG (1969). Determination of coenzyme A and acetyl CoA in tissue extracts. Anal. Biochem 29, 293–299. [PubMed: 4307302]

Arnesen T (2011). Towards a functional understanding of protein N-terminal acetylation. PLoS Biol. 9, e1001074. [PubMed: 21655309]

Ballinger MA, and Andrews MT (2018). Nature's fat-burning machine: brown adipose tissue in a hibernating mammal. J. Exp. Biol 221 (Suppl 1), jeb162586. [PubMed: 29514878]

Bartelt A, Widenmaier SB, Schlein C, Johann K, Goncalves RLS, Eguchi K, Fischer AW, Parlakgul G, Snyder NA, Nguyen TB, et al. (2018). Brown adipose tissue thermogenic adaptation requires Nrf1-mediated proteasomal activity. Nat. Med 24, 292–303. [PubMed: 29400713]

Ben-Sahra I, Howell JJ, Asara JM, and Manning BD (2013). Stimulation of de novo pyrimidine synthesis by growth signaling through mTOR and S6K1. Science 339, 1323–1328. [PubMed: 23429703]

Benador IY, Veliova M, Mahdaviani K, Petcherski A, Wikstrom JD, Assali EA, Acín-Pérez R, Shum M, Oliveira MF, Cinti S, et al. (2018). Mitochondria Bound to Lipid Droplets Have Unique Bioenergetics, Composition, and Dynamics that Support Lipid Droplet Expansion. Cell Metab. 27, 869–885.e6. [PubMed: 29617645]

Benador IY, Veliova M, Liesa M, and Shirihai OS (2019). Mitochondria Bound to Lipid Droplets: Where Mitochondrial Dynamics Regulate Lipid Storage and Utilization. Cell Metab. 29, 827–835. [PubMed: 30905670]

Cannon B, and Nedergaard J (2004). Brown adipose tissue: function and physiological significance. Physiol. Rev 84, 277–359. [PubMed: 14715917]

Chakraborty G, Mekala P, Yahya D, Wu G, and Ledeen RW (2001). Intraneuronal N-acetylaspartate supplies acetyl groups for myelin lipid synthesis: evidence for myelin-associated aspartoacylase. J. Neurochem 78, 736–745. [PubMed: 11520894]

Chouchani ET, Kazak L, and Spiegelman BM (2019). New Advances in Adaptive Thermogenesis: UCP1 and Beyond. Cell Metab. 29, 27–37. [PubMed: 30503034]

Cluntun AA, Lukey MJ, Cerione RA, and Locasale JW (2017). Glutamine Metabolism in Cancer: Understanding the Heterogeneity. Trends Cancer 3, 169–180. [PubMed: 28393116]

Cypess AM, Lehman S, Williams G, Tal I, Rodman D, Goldfine AB, Kuo FC, Palmer EL, Tseng YH, Doria A, et al. (2009). Identification and importance of brown adipose tissue in adult humans. N. Engl. J. Med 360, 1509–1517. [PubMed: 19357406]

Feldmann HM, Golozoubova V, Cannon B, and Nedergaard J (2009). UCP1 ablation induces obesity and abolishes diet-induced thermogenesis in mice exempt from thermal stress by living at thermoneutrality. Cell Metab. 9, 203–209. [PubMed: 19187776]

Fischer AW, Schlein C, Cannon B, Heeren J, and Nedergaard J (2019). Intact innervation is essential for diet-induced recruitment of brown adipose tissue. Am. J. Physiol. Endocrinol. Metab 316, E487–E503. [PubMed: 30576247]

Fromme T, Kleigrewe K, Dunkel A, Retzler A, Li Y, Maurer S, Fischer N, Diezko R, Kanzleiter T, Hirschberg V, et al. (2018). Degradation of brown adipocyte purine nucleotides regulates uncoupling protein 1 activity. Mol. Metab 8, 77–85. [PubMed: 29310935]

Gordon CJ (2012). Thermal physiology of laboratory mice: Defining thermoneutrality. J. Therm. Biol 37, 654–685.

Hankir MK, and Klingenspor M (2018). Brown adipocyte glucose metabolism: a heated subject. EMBO Rep. 19, e46404. [PubMed: 30135070]

Hao Q, Yadav R, Basse AL, Petersen S, Sonne SB, Rasmussen S, Zhu Q, Lu Z, Wang J, Audouze K, et al. (2015). Transcriptome profiling of brown adipose tissue during cold exposure reveals extensive regulation of glucose metabolism. Am. J. Physiol. Endocrinol. Metab 308, E380–E392. [PubMed: 25516548]

Heine M, Fischer AW, Schlein C, Jung C, Straub LG, Gottschling K, Mangels N, Yuan Y, Nilsson SK, Liebscher G, et al. (2018). Lipolysis Triggers a Systemic Insulin Response Essential for Efficient Energy Replenishment of Activated Brown Adipose Tissue in Mice. Cell Metab. 28, 644–655.e4. [PubMed: 30033199]

Held NM, Kuipers EN, van Weeghel M, van Klinken JB, Denis SW, Lombès M, Wanders RJ, Vaz FM, Rensen PCN, Verhoeven AJ, et al. (2018). Pyruvate dehydrogenase complex plays a central role in brown adipocyte energy expenditure and fuel utilization during short-term beta-adrenergic activation. Sci. Rep 8, 9562. [PubMed: 29934543]

Huber K, Hofer DC, Trefely S, Pelzmann HJ, Madreiter-Sokolowski C, Duta-Mare M, Schlager S, Trausinger G, Stryeck S, Graier WF, et al. (2019). N-acetylaspartate pathway is nutrient responsive and coordinates lipid and energy metabolism in brown adipocytes. Biochim. Biophys. Acta Mol. Cell Res 1866, 337–348. [PubMed: 30595160]

Hue L, and Taegtmeyer H (2009). The Randle cycle revisited: a new head for an old hat. Am. J. Physiol. Endocrinol. Metab 297, E578–E591. [PubMed: 19531645]

Hui S, Ghergurovich JM, Morscher RJ, Jang C, Teng X, Lu W, Esparza LA, Reya T, Le Zhan, Yanxiang Guo J, et al. (2017). Glucose feeds the TCA cycle via circulating lactate. Nature 551, 115–118. [PubMed: 29045397]

Hui S, Cowan AJ, Zeng X, Yang L, TeSlaa T, Li X, Bartman C, Zhang Z, Jang C, Wang L, et al. (2020). Quantitative Fluxomics of Circulating Metabolites. Cell Metab. 32, 676–688.e4. [PubMed: 32791100]

Hung CM, Calejman CM, Sanchez-Gurmaches J, Li H, Clish CB, Hettmer S, Wagers AJ, and Guertin DA (2014). Rictor/mTORC2 loss in the Myf5 lineage reprograms brown fat metabolism and protects mice against obesity and metabolic disease. Cell Rep. 8, 256–271. [PubMed: 25001283]

Ikeda K, Kang Q, Yoneshiro T, Camporez JP, Maki H, Homma M, Shinoda K, Chen Y, Lu X, Maretich P, et al. (2017). UCP1-independent signaling involving SERCA2b-mediated calcium cycling regulates beige fat thermogenesis and systemic glucose homeostasis. Nat. Med 23,1454–1465. [PubMed: 29131158]

Isler D, Hill HP, and Meier MK (1987). Glucose metabolism in isolated brown adipocytes under beta-adrenergic stimulation. Quantitative contribution of glucose to total thermogenesis. Biochem. J 245, 789–793. [PubMed: 3311035]

Jang C, Chen L, and Rabinowitz JD (2018). Metabolomics and Isotope Tracing. Cell 173, 822–837. [PubMed: 29727671]

Jung SM, Hung CM, Hildebrand SR, Sanchez-Gurmaches J, Martinez-Pastor B, Gengatharan JM, Wallace M, Mukhopadhyay D, Martinez Calejman C, Luciano AK, et al. (2019). Non-canonical mTORC2 Signaling Regulates Brown Adipocyte Lipid Catabolism through SIRT6-FoxO1. Mol. Cell 75, 807–822.e8. [PubMed: 31442424]

Kazak L, Chouchani ET, Jedrychowski MP, Erickson BK, Shinoda K, Cohen P, Vetrivelan R, Lu GZ, Laznik-Bogoslavski D, Hasenfuss SC, et al. (2015). A creatine-driven substrate cycle enhances energy expenditure and thermogenesis in beige fat. Cell 163, 643–655. [PubMed: 26496606]

Kazak L, Chouchani ET, Lu GZ, Jedrychowski MP, Bare CJ, Mina AI, Kumari M, Zhang S, Vuckovic I, Laznik-Bogoslavski D, et al. (2017). Genetic Depletion of Adipocyte Creatine Metabolism Inhibits Diet-Induced Thermogenesis and Drives Obesity. Cell Metab. 26, 660–671.e3. [PubMed: 28844881]

Kerksick C, and Willoughby D (2005). Theantioxidant role ofglutathioneand N-acetyl-cysteine supplements and exercise-induced oxidative stress. J. Int. Soc. Sports Nutr 2, 38–44. [PubMed: 18500954]

Labbé SM, Caron A, Bakan I, Laplante M, Carpentier AC, Lecomte R, and Richard D (2015). In vivo measurement of energy substrate contribution to cold-induced brown adipose tissue thermogenesis. FASEB J. 29, 2046–2058. [PubMed: 25681456]

Lidell ME, Betz MJ, Dahlqvist Leinhard O, Heglind M, Elander L, Slawik M, Mussack T, Nilsson D, Romu T, Nuutila P, et al. (2013). Evidence for two types of brown adipose tissue in humans. Nat. Med 19, 631–634. [PubMed: 23603813]

Luong A, Hannah VC, Brown MS, and Goldstein JL (2000). Molecular characterization of human acetyl-CoA synthetase, an enzyme regulated by sterol regulatory element-binding proteins. J. Biol. Chem 275, 26458–26466. [PubMed: 10843999]

Lynes MD, Shamsi F, Sustarsic EG, Leiria LO, Wang CH, Su SC, Huang TL, Gao F, Narain NR, Chen EY, et al. (2018). Cold-Activated Lipid Dynamics in Adipose Tissue Highlights a Role for Cardiolipin in Thermogenic Metabolism. Cell Rep. 24, 781–790. [PubMed: 30021173]

Ma SW, and Foster DO (1986). Uptake ofglucose and releaseoffattyacids and glycerol by rat brown adipose tissue in vivo. Can. J. Physiol. Pharmacol 64, 609–614. [PubMed: 3730946]

McCormack JG, and Denton RM (1977). Evidencethatfatty acid synthesis in the interscapular brown adipose tissue of cold-adapted rats is increased in vivo by insulin by mechanisms involving parallel activation of pyruvate dehydrogenase and acetyl-coenzyme A carboxylase. Biochem. J 166, 627–630. [PubMed: 23106]

McDonnell E, Crown SB, Fox DB, Kitir B, Ilkayeva OR, Olsen CA, Grimsrud PA, and Hirschey MD (2016). Lipids Reprogram Metabolism to Become a Major Carbon Source for Histone Acetylation. Cell Rep. 17, 1463–1472. [PubMed: 27806287]

McGarry JD, and Foster DW (1971). The regulation of ketogenesisfrom octanoic acid. The role of the tricarboxylic acid cycle and fatty acid synthesis. J. Biol. Chem 246, 1149–1159. [PubMed: 5543682]

Melamud E, Vastag L, and Rabinowitz JD (2010). Metabolomic analysis and visualization engine for LC-MS data. Anal. Chem 82, 9818–9826. [PubMed: 21049934]

Mottillo EP, Balasubramanian P, Lee YH, Weng C, Kershaw EE, and Granneman JG (2014). Coupling of lipolysis and de novo lipogenesis in brown, beige, and white adipose tissues during chronic β3-adrenergic receptor activation. J. Lipid Res 55, 2276–2286. [PubMed: 25193997]

Nedergaard J, Alexson S, and Cannon B (1980). Cold adaptation in the rat: increased brown fat peroxisomal beta-oxidation relative to maximal mitochondrial oxidative capacity. Am. J. Physiol 239, C208–C216. [PubMed: 7435608]

Nedergaard J, Bengtsson T, and Cannon B (2007). Unexpected evidence for active brown adipose tissue in adult humans. Am. J. Physiol. Endocrinol. Metab 293, E444–E452. [PubMed: 17473055]

Nedergaard J, Bengtsson T, and Cannon B (2011). New powers of brown fat: fighting the metabolic syndrome. Cell Metab. 13, 238–240. [PubMed: 21356513]

Olsen JM, Csikasz RI, Dehvari N, Lu L, Sandström A, Öberg AI, Nedergaard J, Stone-Elander S, and Bengtsson T (2017). β_3-Adrenergically induced glucose uptake in brown adiposetissue is independent of UCP1 presence or activity: Mediation through the mTOR pathway. Mol. Metab 6, 611–619. [PubMed: 28580291]

Ouellet V, Labbé SM, Blondin DP, Phoenix S, Guérin B, Haman F, Turcotte EE, Richard D, and Carpentier AC (2012). Brown adipose tissue oxidative metabolism contributes to energy expenditure during acute cold exposure in humans. J. Clin. Invest 122, 545–552. [PubMed: 22269323]

Panic V, Pearson S, Banks J, Tippetts TS, Velasco-Silva JN, Lee S, Simcox J, Geoghegan G, Bensard CL, van Ry T, et al. (2020). Mitochondrial pyruvate carrier is required for optimal brown fat thermogenesis. eLife 9, e52558. [PubMed: 32795388]

Pessentheiner AR, Pelzmann HJ, Walenta E, Schweiger M, Groschner LN, Graier WF, Kolb D, Uno K, Miyazaki T, Nitta A, et al. (2013). NAT8L (N-acetyltransferase 8-like) accelerates lipid turnover and increases energy expenditure in brown adipocytes. J. Biol. Chem 288, 36040–36051. [PubMed: 24155240]

Prokesch A, Pelzmann HJ, Pessentheiner AR, Huber K, Madreiter-So-kolowski CT, Drougard A, Schittmayer M, Kolb D, Magnes C, Trausinger G, et al. (2016). N-acetylaspartate catabolism determines cytosolic acetyl-CoA levels and histone acetylation in brown adipocytes. Sci. Rep 6, 23723. [PubMed: 27045997]

Ramirez AK, Lynes MD, Shamsi F, Xue R, Tseng YH, Kahn CR, Kasif S, and Dreyfuss JM (2017). Integrating Extracellular Flux Measurements and Genome-Scale Modeling Reveals Differences between Brown and White Adipocytes. Cell Rep. 21, 3040–3048. [PubMed: 29241534]

Rothwell NJ, and Stock MJ (1979). A role for brown adipose tissue in diet-induced thermogenesis. Nature 281, 31–35. [PubMed: 551265]

Saggerson ED, McAllister TW, and Baht HS (1988). Lipogenesis in rat brown adipocytes. Effects of insulin and noradrenaline, contributions from glucose and lactate as precursors and comparisons with white adipocytes. Biochem. J 251, 701–709. [PubMed: 3137922]

Saito M, Okamatsu-Ogura Y, Matsushita M, Watanabe K, Yoneshiro T, Nio-Kobayashi J, Iwanaga T, Miyagawa M, Kameya T, Nakada K, et al. (2009). High incidence of metabolically active brown adipose tissue in healthy adult humans: effects of cold exposure and adiposity. Diabetes 58, 1526–1531. [PubMed: 19401428]

Salvatore D, Bartha T, and Larsen PR (1998). The guanosine monophosphate reductase gene is conserved in rats and its expression increases rapidly in brown adipose tissue during cold exposure. J. Biol. Chem 273, 31092–31096. [PubMed: 9813009]

Sanchez-Gurmaches J, Hung CM, and Guertin DA (2016). Emerging Complexities in Adipocyte Origins and Identity. Trends Cell Biol. 26, 313–326. [PubMed: 26874575]

Sanchez-Gurmaches J, Tang Y, Jespersen NZ, Wallace M, Martinez Calejman C, Gujja S, Li H, Edwards YJK, Wolfrum C, Metallo CM, et al. (2018). Brown Fat AKT2 Is a Cold-Induced Kinase that Stimulates ChREBPMediated De Novo Lipogenesis to Optimize Fuel Storage and Thermogenesis. Cell Metab. 27, 195–209.e6. [PubMed: 29153407]

Scheele C, and Wolfrum C (2020). Brown Adipose Crosstalk in Tissue Plasticity and Human Metabolism. Endocr. Rev 41, 53–65.

Shabalina IG, and Nedergaard J (2011). Mitochondrial (‘mild’) uncoupling and ROS production: physiologically relevant or not? Biochem. Soc. Trans 39, 1305–1309. [PubMed: 21936806]

Shimazu T, and Takahashi A (1980). Stimulation of hypothalamic nuclei has differential effectson lipid synthesis in brown and white adipose tissue. Nature 284, 62–63. [PubMed: 6444457]

Song A, Dai W, Jang MJ, Medrano L, Li Z, Zhao H, Shao M, Tan J, Li A, Ning T, et al. (2020). Low- and high-thermogenic brown adipocyte subpopulations coexist in murine adipose tissue. J. Clin. Invest 130, 247–257. [PubMed: 31573981]

Straub LG, Efthymiou V, Grandl G, Balaz M, Challa TD, Truscello L, Horvath C, Moser C, Rachamin Y, Arnold M, et al. (2019). Antioxidants protect against diabetes by improving glucose homeostasis in mouse models of inducible insulin resistance and obesity. Diabetologia 62, 2094–2105. [PubMed: 31309261]

Su X, Lu W, and Rabinowitz JD (2017). Metabolite Spectral Accuracy on Orbitraps. Anal. Chem 89, 5940–5948. [PubMed: 28471646]

Sun W, Dong H, Balaz M, Slyper M, Drokhlyansky E, Colleluori G, Giordano A, Kovanicova Z, Stefanicka P, Ding L, et al. (2020). Single-nucleus RNA-Seq reveals a new type of brown adipocyte regulating thermogenesis. bioRxiv. 10.1101/2020.01.20.890327.

Sustarsic EG, Ma T, Lynes MD, Larsen M, Karavaeva I, Havelund JF, Nielsen CH, Jedrychowski MP, Moreno-Torres M, Lundh M, et al. (2018). Cardiolipin Synthesis in Brown and Beige Fat Mitochondria Is Essential for Systemic Energy Homeostasis. Cell Metab. 28, 159–174.e11. [PubMed: 29861389]

Tanner LB, Goglia AG, Wei MH, Sehgal T, Parsons LR, Park JO, White E, Toettcher JE, and Rabinowitz JD (2018). Four Key Steps Control Glycolytic Flux in Mammalian Cells. Cell Syst. 7, 49–62.e8. [PubMed: 29960885]

Townsend KL, and Tseng YH (2015). Of mice and men: novel insights regarding constitutive and recruitable brown adipocytes. Int. J. Obes. Suppl 5 (Suppl 1), S15–S20. [PubMed: 27152169]

Trayhurn P (1979). Fatty acid synthesis in vivo in brown adipose tissue, liver and white adipose tissue of the cold-acclimated rat. FEBS Lett. 104, 13–16. [PubMed: 477972]

Trayhurn P (1981). Fatty acid synthesis in mouse brown adipose tissue. The influence of environmental temperature on the proportion of whole-body fatty acid synthesis in brown adipose tissue and the liver. Biochim. Biophys. Acta 664, 549–560. [PubMed: 7272321]

van Marken Lichtenbelt WD, Vanhommerig JW, Smulders NM, Drossaerts JM, Kemerink GJ, Bouvy ND, Schrauwen P, and Teule GJ (2009). Cold-activated brown adipose tissue in healthy men. N. Engl. J. Med 360, 1500–1508. [PubMed: 19357405]

Virtanen KA, Lidell ME, Orava J, Heglind M, Westergren R, Niemi T, Taittonen M, Laine J, Savisto NJ, Enerback S, and Nuutila P (2009). Functional brown adipose tissue in healthy adults. N. Engl. J. Med 360, 1518–1525. [PubMed: 19357407]

von Essen G, Lindsund E, Cannon B, and Nedergaard J (2017). Adaptive facultative diet-induced thermogenesis in wild-type but not in UCP1-ablated mice. Am. J. Physiol. Endocrinol. Metab 313, E515–E527. [PubMed: 28679625]

Wakil SJ, and Abu-Elheiga LA (2009). Fatty acid metabolism: target for metabolic syndrome. J. Lipid Res 50 (Suppl), S138–S143. [PubMed: 19047759]

Wang Z, Ning T, Song A, Rutter J, Wang QA, and Jiang L (2020). Chronic cold exposure enhances glucose oxidation in brown adipose tissue. EMBO Rep. 21, e50085. [PubMed: 33043581]

Weir G, Ramage LE, Akyol M, Rhodes JK, Kyle CJ, Fletcher AM, Craven TH, Wakelin SJ, Drake AJ, Gregoriades ML, et al. (2018). Substantial MetabolicActivity ofHuman Brown Adipose Tissue during Warm Conditions and Cold-Induced Lipolysis of Local Triglycerides. Cell Metab. 27, 1348–1355.e4. [PubMed: 29805098]

Williams L, Burgos ES, Vuguin PM, Manuel CR, Pekson R, Munnangi S, Reznik SE, and Charron MJ (2019). N-Acetylcysteine Resolves Placental Inflammatory-Vasculopathic Changes in Mice Consuming a High-Fat Diet. Am. J. Pathol 189, 2246–2257. [PubMed: 31430466]

Winther S, Isidor MS, Basse AL, Skjoldborg N, Cheung A, Quistorff B, and Hansen JB (2018). Restricting glycolysis impairs brown adipocyte glucose and oxygen consumption. Am. J. Physiol. Endocrinol. Metab 314, E214–E223. [PubMed: 29118013]

Wollenberger A, Ristau O, and Schoffa G (1960). [A simple technic for extremely rapid freezing of large pieces of tissue]. Pflugers Arch. Gesamte Physiol. Menschen Tiere 270, 399–412.

Yoo H, Antoniewicz MR, Stephanopoulos G, and Kelleher JK (2008). Quantifying reductive carboxylation flux of glutamine to lipid in a brown adipocyte cell line. J. Biol. Chem 283, 20621–20627. [PubMed: 18364355]

Yu XX, Lewin DA, Forrest W, and Adams SH (2002). Cold elicits the simultaneous induction of fatty acid synthesis and beta-oxidation in murine brown adipose tissue: prediction from differential gene expression and confirmation in vivo. FASEB J. 16, 155–168. [PubMed: 11818363]

Yu J, Zhang S, Cui L, Wang W, Na H, Zhu X, Li L, Xu G, Yang F, Christian M, and Liu P (2015). Lipid droplet remodeling and interaction with mitochondria in mouse brown adipose tissue during cold treatment. Biochim. Biophys. Acta 1853, 918–928.

Highlights

- *In vivo* BAT glucose fluxes vary with the degree and duration of cold exposure
- BAT uses glucose to support auxiliary pathways beyond glycolysis and the TCA cycle
- Cold-adapted BAT rapidly synthesizes fatty acids *de novo* for acyl-carnitine production
- *N*-acetylated amino acids are markers of thermogenesis

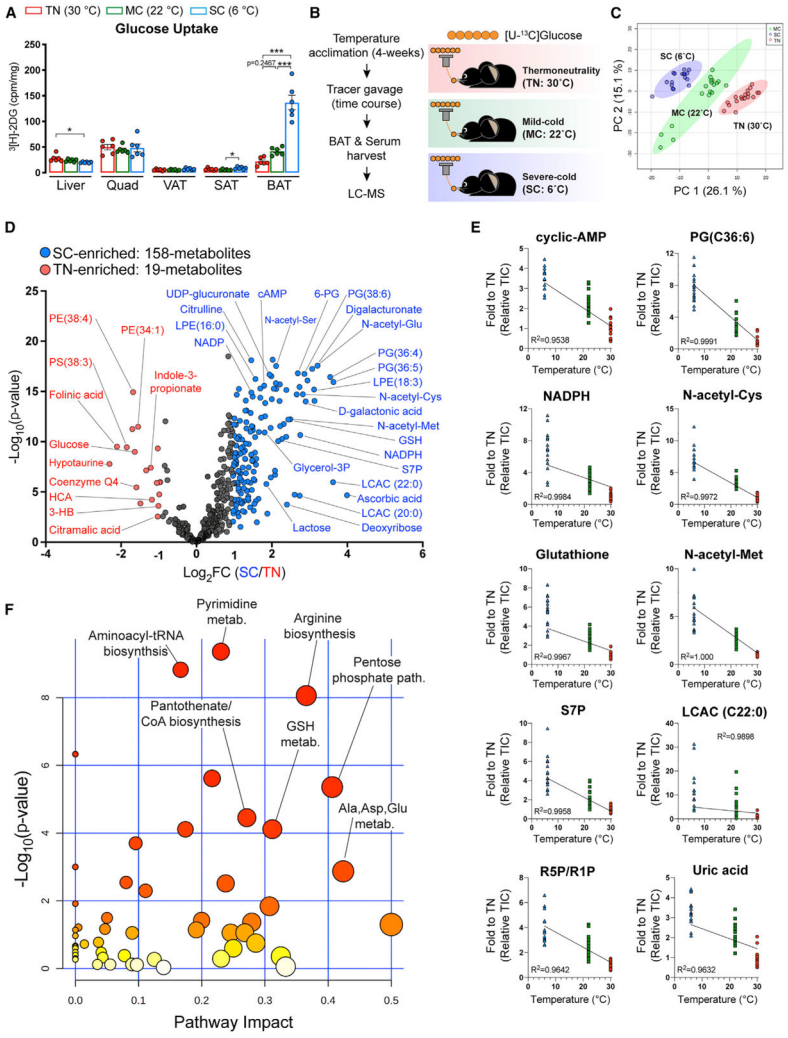

Figure 1. Severe cold (SC) profoundly remodels BAT's metabolic landscape

(A) Uptake of orally delivered ^{3}H-2-deoxy-glucose (^{3}H-2DG) by the indicated organs in mice acclimated to thermoneutrality (TN; red, 30°C), mild cold (MC; green, 22°C), and SC (blue, 6°C) for 4 weeks (n = 6). For subcutaneous adipose tissue (SAT) and visceral adipose tissue (VAT), inguinal WAT and perigonadal WAT were collected, respectively.

(B) Experimental strategy for *in vivo* isotope tracing and metabolomics of BAT in mice adapted to different temperatures. Mice were acclimated to TN, MC, and SC for 4 weeks. Then, mice received [U-^{13}C]-glucose tracer via oral gavage. Metabolite levels, labeling in serum, and BAT were measured at multiple time points after gavage by LC-MS (n = 5–7 per time point).

(C) Principal-component analysis (PCA) of BAT metabolome in mice adapted to TN, MC, and SC (n = 17–20).

(D) Volcano plot of BAT metabolome in mice adapted to TN versus SC. The colored dots (blue or red) indicate significantly enriched metabolites at each group ($1 \geq \text{Log}_2$ fold changes compared with counterpart, $p < 0.05$ after false discovery rate [FDR] correction) (n = 17–20).

(E) Metabolites showing a linear relationship between temperatures and fold change of pool size normalized to TN.
(F) Metabolic pathway analysis of BAT metabolome in mice adapted to TN versus SC. The top pathways are ranked by the adjusted p values for permutation per pathway (y axis) and the total number of hits per pathway (x axis). The color graduated from white to yellow, orange, and red; circle size (from small to large) and the increase in values of both x and y represent the degree of significance.
TIC, total ion count.

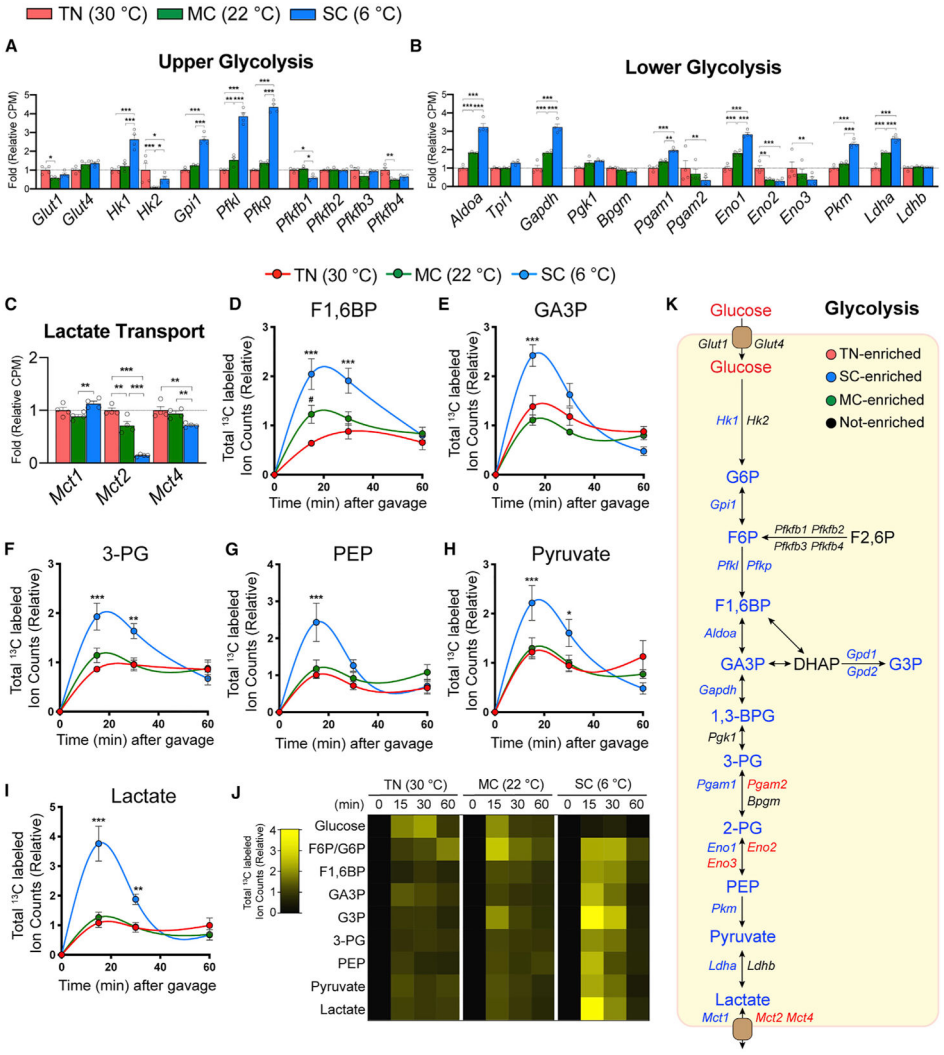

Figure 2. Integrative transcriptomics and metabolic tracing analysis reveal increased BAT glycolytic flux upon SC

(A–C) Relative gene levels of upper or lower glycolytic enzymes and glucose or lactate transporters in BAT from mice acclimated to TN (red, 30°C), MC (green, 22°C), and SC (SC; blue, 6°C) for 4 weeks, measured by RNA sequencing (n = 4).

(D–I) Total labeled carbons in the indicated glycolytic intermediates of BAT (n = 5–7).

(J) Heatmap showing relative total labeled carbons in the indicated glycolytic metabolites (n = 5–7).

(K) Glycolysis pathway. Colors indicate a temperature group showing significantly higher labeling or transcript abundance than other groups.

Data are mean ± SEM. Statistical significance was calculated using two-way ANOVA with Tukey's multiple comparison test: *,#$p < 0.05$; **,##$p < 0.01$; ***,###$p < 0.001$ (TN versus SC, TN versus MC).

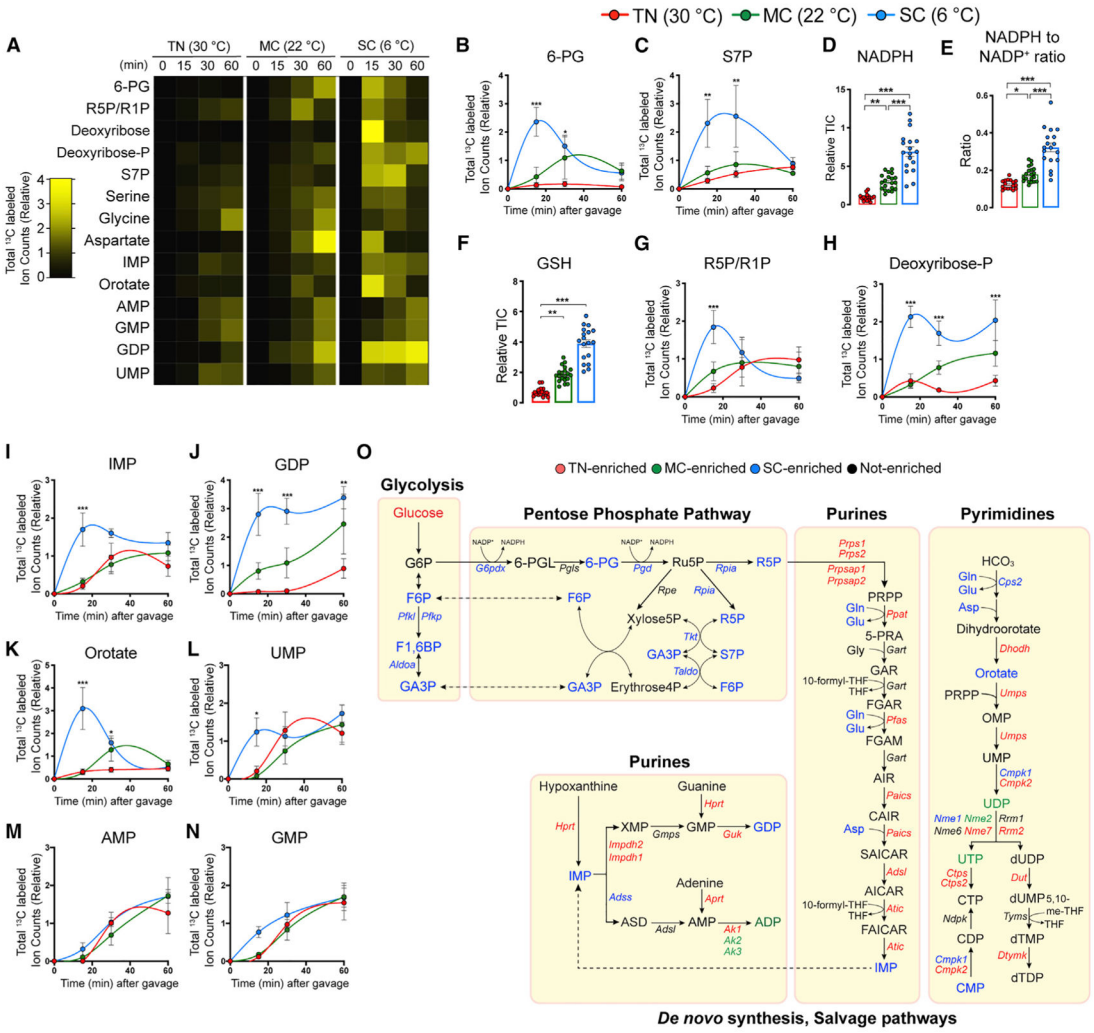

Figure 3. SC triggers BAT glucose flux into the pentose phosphate pathway that contributes to antioxidant and nucleotide synthesis

(A) Heatmap showing relative total labeled carbons in the BAT metabolic intermediates in the pentose-phosphate pathway, nucleotides, and key amino acids in nucleotide biosynthesis from mice acclimated to TN (30°C), MC (22°C), and SC (6°C) for 4 weeks followed by fed [U-^{13}C]-glucose via oral gavage (n = 5–7).

(B and C) Total labeled carbons in the pentose phosphate pathway intermediates of BAT (TN: red, 30°C; MC: green, 22°C; SC: blue, 6°C; n = 5–7).

(D) Relative abundance of total NADPH of BAT (n = 17–20).

(E) Relative abundance of NADPH over NADP$^+$ of BAT (n = 17–20).

(F) Relative abundance of total glutathione (GSH) of BAT (n = 17–20).

(G and H) Total labeled carbons in the ribose phosphate species of BAT (n = 5–7).

(I–N) Total labeled carbons in the purine/pyrimidine biosynthesis intermediates of BAT (n = 5–7).

(O) Branch pathways of glycolysis, including pentose phosphate pathway and nucleotide, glycogen, and hexosamine biosynthesis and nucleotide-sugar pathways.

Data are mean ± SEM. Statistical significance was calculated using two-way ANOVA with Tukey's multiple comparison test: $^{*,\#}p < 0.05$; $^{**,\#\#}p < 0.01$; $^{***,\#\#\#}p < 0.001$ (TN versus SC, TN versus MC).

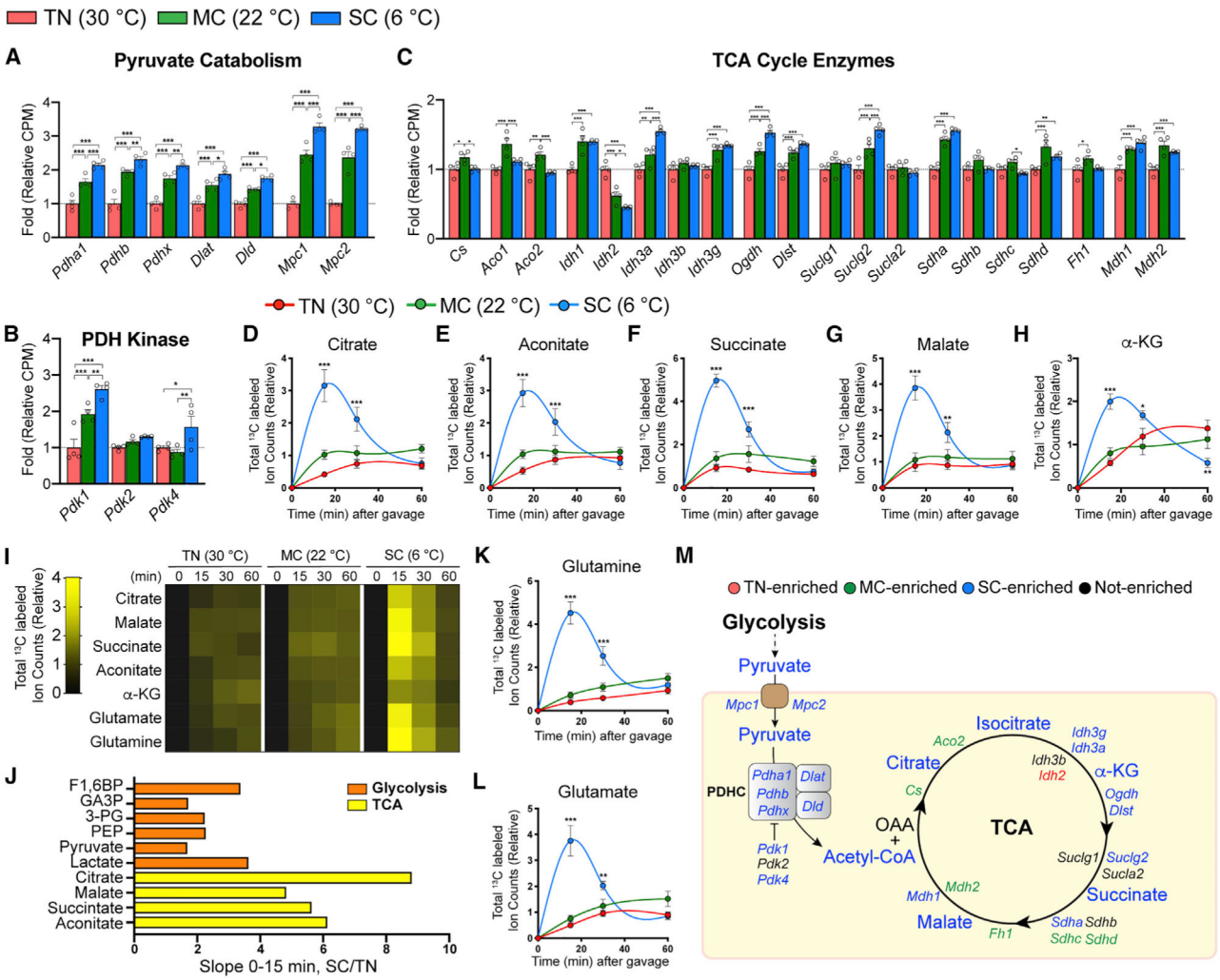

Figure 4. SC, but not MC, increases glucose flux into the TCA cycle

(A–C) Relative gene levels of pyruvate catabolism and transporters, PDH kinases, and TCA cycle enzymes in BAT from mice acclimated to TN (red, 30°C), MC (green, 22°C), or SC (blue, 6°C) for 4 weeks, measured by RNA sequencing (n = 4).

(D–H) Total labeled carbons in the TCA intermediates of BAT from mice acclimated to TN, MC, and SC for 4 weeks, followed by [U-^{13}C]-glucose provision via oral gavage (n = 5–7).

(I) Heatmap showing relative total labeled carbons in the TCA intermediates of BAT (n = 5–7).

(J) Bar graph showing each metabolite's relative slope$_{(0\text{-}15\ min)}$ of SC over TN.

(K and L) Total labeled carbons in glutamine (K) and glutamate (L) of BAT (n = 5–7).

(M) TCA cycle map. Colors indicate a temperature group showing significantly higher labeling or transcript abundance than other groups.

Data are mean ± SEM. Statistical significance was calculated using two-way ANOVA with Tukey's multiple comparison test: *,$^{\#}$p < 0.05; **,$^{\#\#}$p < 0.01; ***,$^{\#\#\#}$p < 0.001 (TN versus SC, TN versus MC).

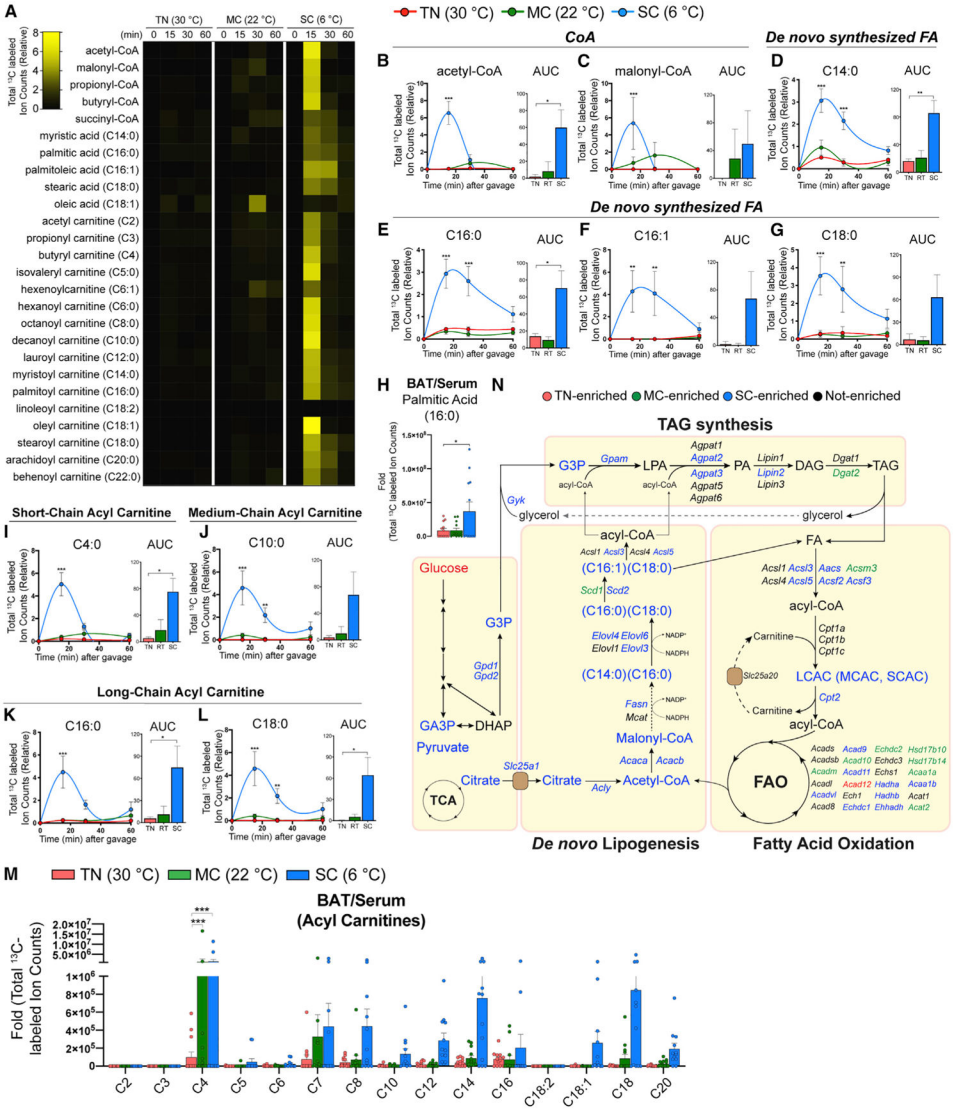

Figure 5. BAT glucose usage for fatty acid synthesis and oxidation is accelerated by SC, but not by MC

(A) Heatmap showing relative total labeled carbons of fatty acids and their precursors and acyl-carnitine species in BAT from mice acclimated to TN (30°C), MC (22°C), and SC (6°C) for 4 weeks, followed by [U-^{13}C]-glucose provision via oral gavage (n = 5–7).

(B and C) Total labeled carbons in the CoA species of BAT and their area under curve ($AUC_{0–60\ min}$) (TN: red, 30°C; MC: green, 22°C; SC: blue, 6°C; n = 5–7).

(D–G) Total labeled carbons in the fatty acids of BAT and their $AUC_{0–60\ min}$ (n = 5–7).

(H) Relative total labeled carbons in palmitic acid of BAT over serum (n = 12–13).

(I–L) Total labeled carbons in the acyl carnitines of BAT and their $AUC_{0–60\ min}$ (n = 5–7).

(M) Relative total labeled carbons in the acyl carnitine species of BAT over serum (n = 12–13).

(N) Pathway map of *de novo* lipogenesis, triacylglycerol (TAG) synthesis, and fatty acid oxidation. Colors indicate a temperature group showing significantly higher labeling or transcript abundance than other groups.

Data are mean ± SEM. Statistical significance was calculated using two-way ANOVA with Tukey's multiple comparison test: $^{*,\#}p < 0.05$; $^{**,\#\#}p < 0.01$; $^{***,\#\#\#}p < 0.001$ (TN versus SC, TN versus MC).

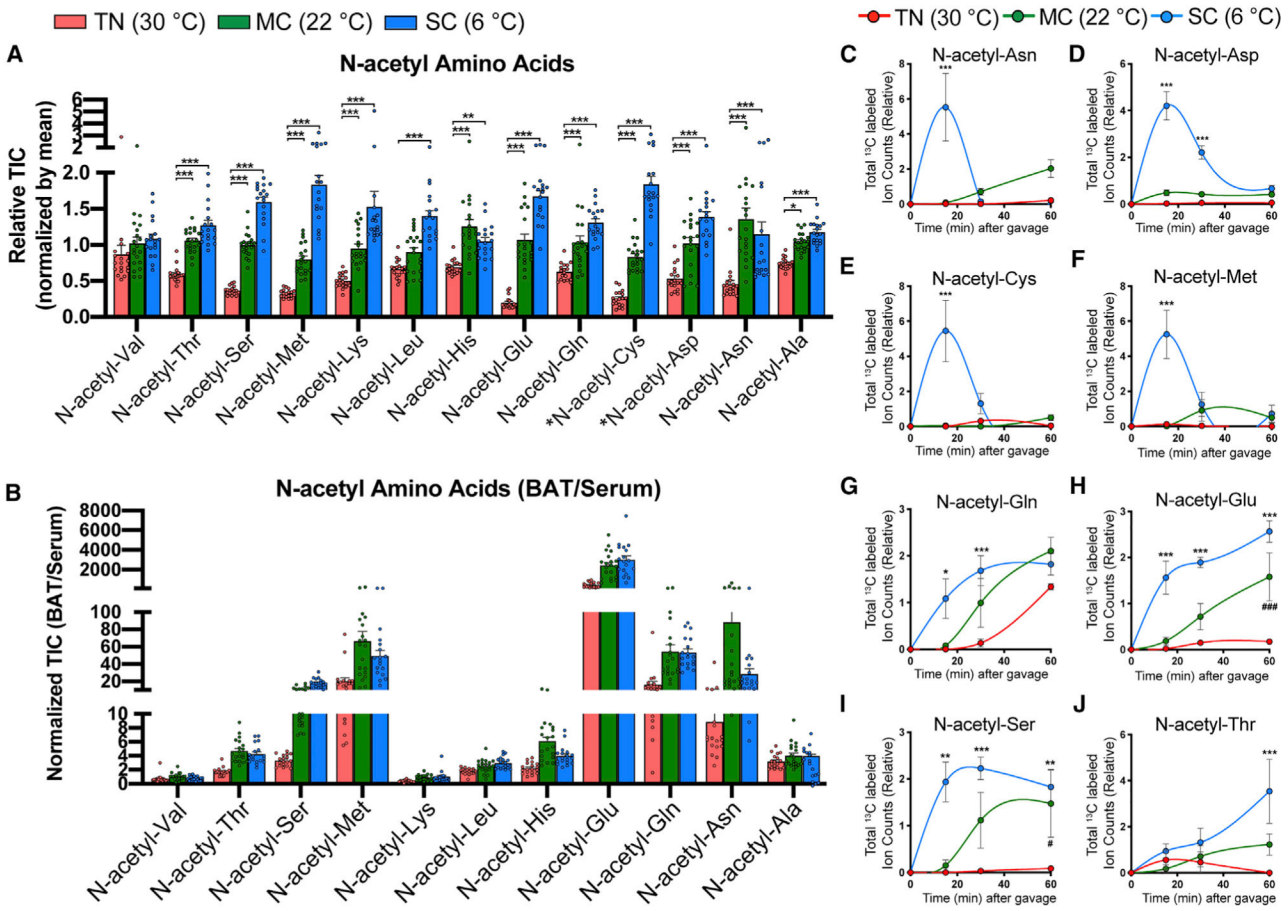

Figure 6. *N*-acetyl-amino acids are highly enriched and produced in BAT upon cold

(A) Relative abundance of N-acetyl-amino acids in BAT from mice acclimated to TN (red, 30°C), MC (green, 22°C), and SC (blue, 6°C) for 4 weeks, followed by [U-^{13}C]-glucose provision via oral gavage (n = 17–20). *Note that *N*-acetyl-cysteine (N-acetyl-Cys) and *N*-acetyl-aspartate (N-acetyl-Asp) were detected only within BAT, but not in serum.

(B) Relative abundance of *N*-acetyl-amino acids in BAT over serum (n = 17–20).

(C–J) Total labeled carbons in the N-acetyl-amino acids of BAT (n = 5–7).

Data are mean ± SEM. Statistical significance was calculated using two-way ANOVA with Tukey's multiple comparison test: *,$^{\#}$p < 0.05; **,$^{\#\#}$p < 0.01; ***,$^{\#\#\#}$p < 0.001 (TN versus SC, TN versus MC).

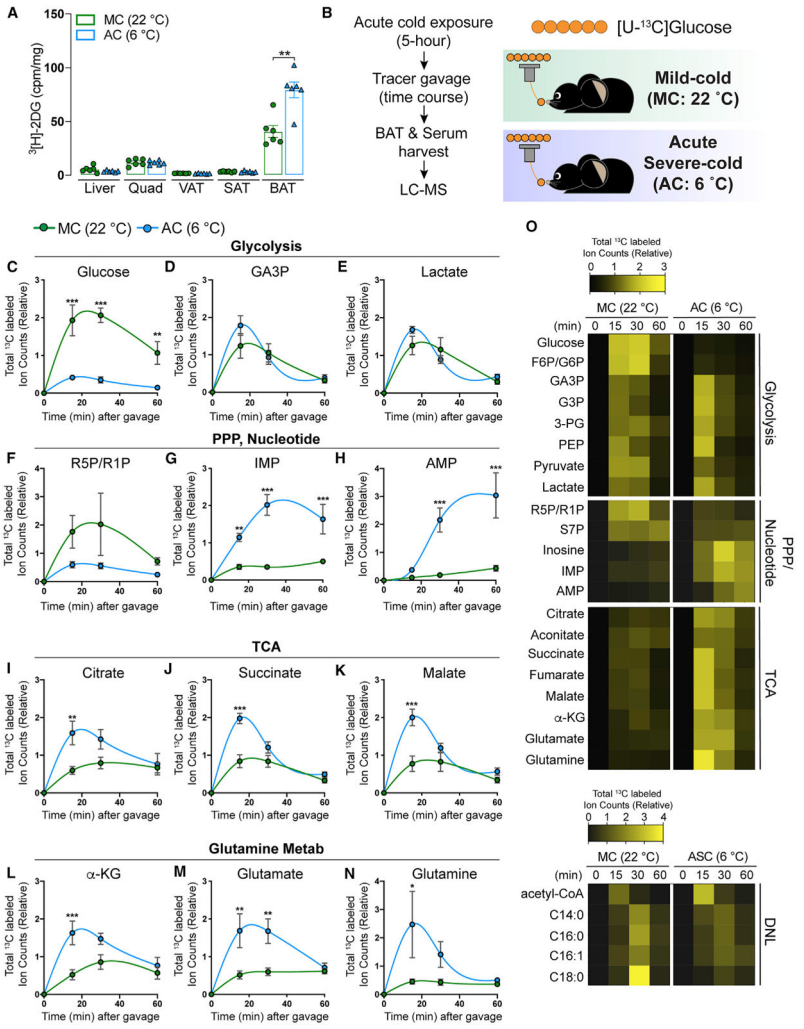

Figure 7. Acute cold increases glucose flux into glycolysis, TCA cycle, and pentose phosphate pathway, but not *de novo* fatty acid synthesis

(A) Uptake of orally delivered ^{3}H-2DG by the indicated organs in mice acutely challenged with SC (AC: blue, 6°C, 5 h) or acclimated to standard room temperature conditions, which is MC for mice (MC: green, 22°C) (n = 6). For SAT and VAT, inguinal WAT and perigonadal WAT were collected, respectively.

(B) Experimental strategy for *in vivo* isotope tracing and metabolomics of BAT in mice acutely challenged with SC. Mice were exposed to SC for 5 h (AC: blue, 6°C). As a control, mice acclimated to MC (green, 22°C) were used. Then, mice received [U-^{13}C]-glucose tracer via oral gavage. Metabolite levels, labeling in serum, and BAT were measured at multiple time points after gavage by LC-MS (n = 6–8 per time point).

(C–E) Total labeled carbons in the glycolytic intermediates of BAT samples from mice acutely exposed to AC and their counterpart (MC) followed by feeding with [U-^{13}C]-glucose via oral gavage (n = 6–8).

(F–H) Total labeled carbons in the pentose phosphate pathway and nucleotide biosynthesis of BAT (n = 6–8).

(I–K) Total labeled carbons in the TCA intermediates of BAT (n = 6–8).

(L–N) Total labeled carbons in α-ketoglutarate (L), glutamate (M), and glutamine (N) (n = 6–8).

(O) Heatmap showing relative total labeled carbons in the indicated metabolites (n = 6–8). Data are mean ± SEM. Statistical significance was calculated using two-way ANOVA with Tukey's multiple comparison test: $^{*,\#}p < 0.05$; $^{**,\#\#}p < 0.01$; $^{***,\#\#\#}p < 0.001$ (TN versus SC, TN versus MC).

KEY RESOURCES TABLE

REAGENT or RESOURCE	SOURCE	IDENTIFIER
Antibodies		
Raptor	Cell Signaling Technology	Cat# 2280; RRID: AB_561245
ACC	Cell Signaling Technology	Cat# 3676; RRID: AB_2219397
ACLY	Cell Signaling Technology	Cat# 4332; RRID: AB_2223744
FASN	Cell Signaling Technology	Cat# 3180; RRID: AB_2100796
α-Tubulin	Cell Signaling Technology	Cat# 2125; RRID: AB_2619646
PPARγ	Santa Cruz biotechnology	Cat# sc-7273; RRID: AB_628115
UCP1	Abcam	Cat# ab10983; RRID: AB_2241462
Chemicals, peptides, and recombinant proteins		
D-GLUCOSE (U-13C6, 99%)	Cambridge Isotope Laboratories	Cat#CLM-1396-PK
[1,2-^{3}H]-deoxy-D-glucose	Perkin Elmer	NET328A001MC
Critical commercial assays		
Glucose meter	Bionime	GE100
Ultrasensitive insulin ELISA kit	Crystal Chem	90060
Deposited data		
Data S1. Isotope tracing and Metabolomics upon temperature acclimation, related to Figures 1, 2, 3, 4, 5, 6, and S1-S9	This Study	Supplemental information
Data S2. Isotope tracing and Metabolomics upon acute cold, related to Figures 7 and S10	This Study	Supplemental information
RNA sequencing raw data upon temperature acclimation, related to Figures 2, 4, S3-S5, S7, and S8	Sanchez-Gurmaches et al., 2018 (PMID: 29153407)	NCBI Gene Expression Omnibus: GSE96681
Experimental models: Organisms/Strains		
Mouse: C57BL/6	Jackson labs	000664
Software and algorithms		
Graphpad	GraphPad Software	Graphpad.com
Adobe Illustrator	Adobe	Adobe.com
MAVEN software	http://genomics-pubs.princeton.edu/mzroll/index.php	N/A
MetaboAnalyst 3.0, 4.0, 5.0	https://www.metaboanalyst.ca	N/A
Other		
Rodent incubators	Power Scientific	RIT33SD